Article

Molecular Cell

Distinct tRNA Accommodation Intermediates Observed on the Ribosome with the Antibiotics Hygromycin A and A201A

Graphical Abstract

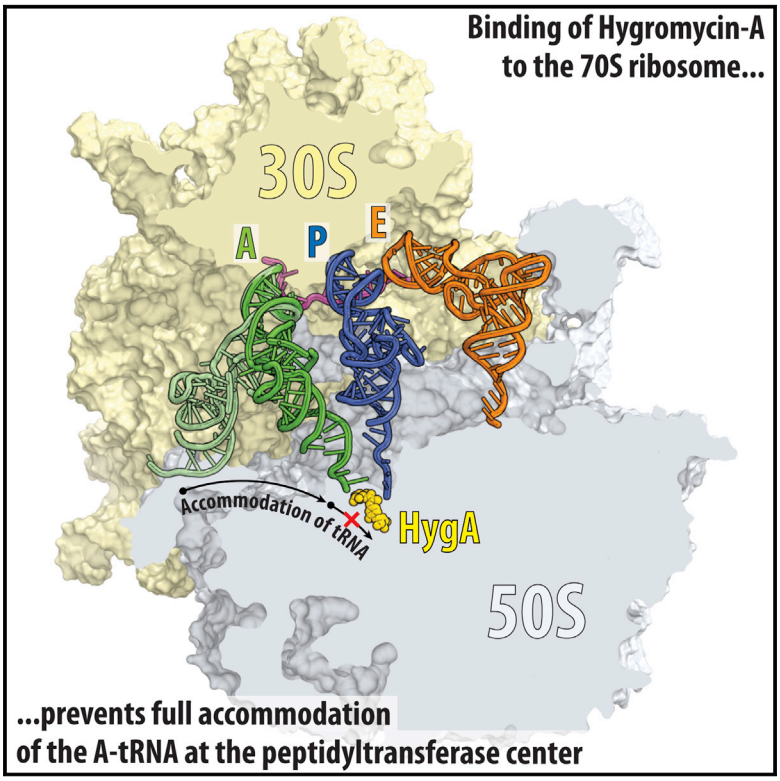

Highlights

- X-ray structures of antibiotics Hygromycin A and A201A on the ribosome
- Structural basis for Hygromycin A and A201A resistance mechanisms
- tRNA accommodation intermediates with Hygromycin A/A201A observed by FRET
- X-ray structures of partially accommodated A-tRNAs with Hygromycin A/A201A

Authors

Yury S. Polikanov, Agata L. Starosta, ..., Thomas A. Steitz, Daniel N. Wilson

Correspondence

scb2005@med.cornell.edu (S.C.B.), thomas.steitz@yale.edu (T.A.S.), wilson@lmb.uni-muenchen.de (D.N.W.)

In Brief

The increase in multi-drug-resistant bacteria has prompted a renewed interest in antibiotics with novel chemical scaffolds. Polikanov et al. report a structural and biochemical analysis of the ribosome-target antibiotics hygromycin A and A201A and reveal their binding site and mechanism of action to inhibit tRNA accommodation during translation.

Polikanov et al., 2015, Molecular Cell *58*, 832–844
June 4, 2015
http://dx.doi.org/10.1016/j.molcel.2015.04.014

CellPress

Molecular Cell
Article

Distinct tRNA Accommodation Intermediates Observed on the Ribosome with the Antibiotics Hygromycin A and A201A

Yury S. Polikanov,[1,2,9] Agata L. Starosta,[3,9] Manuel F. Juette,[4,9] Roger B. Altman,[4] Daniel S. Terry,[4] Wanli Lu,[5] Benjamin J. Burnett,[4] George Dinos,[6] Kevin A. Reynolds,[5] Scott C. Blanchard,[4,7,*] Thomas A. Steitz,[1,2,*] and Daniel N. Wilson[3,8,*]

[1]Department of Molecular Biophysics and Biochemistry, Yale University, New Haven, CT 06520, USA
[2]Howard Hughes Medical Institute, Chevy Chase, MD 20815, USA
[3]Gene Center and Department for Biochemistry, University of Munich, Feodor-Lynenstr. 25, 81377 Munich, Germany
[4]Department of Physiology and Biophysics, Weill Medical College of Cornell University, New York, NY 10065, USA
[5]Department of Chemistry, Portland State University, Portland, OR 97207, USA
[6]Department of Biochemistry, School of Medicine, University of Patras, 26500 Patras, Greece
[7]Tri-Institutional Training Program in Chemical Biology, New York, NY 10065, USA
[8]Center for integrated Protein Science Munich (CiPSM), University of Munich, Feodor-Lynenstr. 25, 81377 Munich, Germany
[9]Co-first author
*Correspondence: scb2005@med.cornell.edu (S.C.B.), thomas.steitz@yale.edu (T.A.S.), wilson@lmb.uni-muenchen.de (D.N.W.)
http://dx.doi.org/10.1016/j.molcel.2015.04.014

SUMMARY

The increase in multi-drug-resistant bacteria is limiting the effectiveness of currently approved antibiotics, leading to a renewed interest in antibiotics with distinct chemical scaffolds. We have solved the structures of the *Thermus thermophilus* 70S ribosome with A-, P-, and E-site tRNAs bound and in complex with either the aminocyclitol-containing antibiotic hygromycin A (HygA) or the nucleoside antibiotic A201A. Both antibiotics bind at the peptidyl transferase center and sterically occlude the CCA-end of the A-tRNA from entering the A site of the peptidyl transferase center. Single-molecule Förster resonance energy transfer (smFRET) experiments reveal that HygA and A201A specifically interfere with full accommodation of the A-tRNA, leading to the presence of tRNA accommodation intermediates and thereby inhibiting peptide bond formation. Thus, our results provide not only insight into the mechanism of action of HygA and A201A, but also into the fundamental process of tRNA accommodation during protein synthesis.

INTRODUCTION

The process of protein synthesis in a bacterial cell is one of the major targets for antibiotics, with more than half of clinically used drugs binding to the ribosome (Wilson, 2009, 2014). However, the increase in multi-drug resistance within many pathogenic bacteria has limited the utility of many of the currently available antibiotics, which has renewed interest in the discovery and characterization of small-molecule compounds with novel chemical scaffolds (Sutcliffe, 2011). Two such compounds are hygromycin A (HygA, Figure 1A) and A201A (Figure 1B), which bear some resemblance to each other, as well as to the well-characterized nucleoside antibiotic puromycin (PMN) (Figure 1C).

HygA was first discovered in the 1950s as a secondary metabolite produced by *Streptomyces hygroscopicus* (Mann et al., 1953; Pittenger et al., 1953). Biosynthetic studies have revealed that HygA is assembled from three independently synthesized subunits, 5-dehydro-α-L-fucofuranose (subunit A), (E)-3-(3,4-dihydroxyphenyl)-2-methylacrylic acid (subunit B), and the aminocyclitol, 2L-2-amino-2-deoxy-4,5-O-methylene-neo-inositol (subunit C) (Kakinuma et al., 1976; Mann and Woolf, 1957) (Figure 1A). HygA is, therefore, structurally distinct from the well-characterized aminoglycoside antibiotic hygromycin B, which was subsequently isolated from the same organism (Mann and Bromer, 1958). HygA has broad-spectrum activity against Gram-positive and, to a lesser extent, Gram-negative bacteria (Hayashi et al., 1997; Mann et al., 1953; Wakisaka et al., 1980). HygA also displays strong in vitro potency against *Serpulina* (*Treponema*) *hyodysenteriae* (Nakagawa et al., 1987; Omura et al., 1987), the causative agent of swine dysentery, an economically significant muco-hemorrhagic disease of pigs. In addition, HygA and its derivatives have been reported to have herbicidal (Kim et al., 1990; Lee et al., 2003) as well as immunosuppressant properties (Uyeda et al., 2001; Yoshida et al., 1986). Biochemical studies indicate that HygA inhibits translation by binding to the peptidyl transferase center (PTC) on the large ribosomal subunit and preventing the binding of aminoacyl-tRNA (aa-tRNA) to the A site (Guerrero and Modolell, 1980; Polacek et al., 2002; Poulsen et al., 2000).

A201A is an aminoacyl-nucleoside antibiotic that was first isolated from *Streptomyces capreolus* NRRL 3817 (Kirst et al., 1985) and more recently from the deep-sea marine actinomycete *Marinactinospora thermotolerans* SCSIO 00652 (Zhu et al., 2012). A201A is comprised of five subunits (Figure 1B): 6-N-dimethylaminopurine (A), 3′-amino-3′-deoxyribose

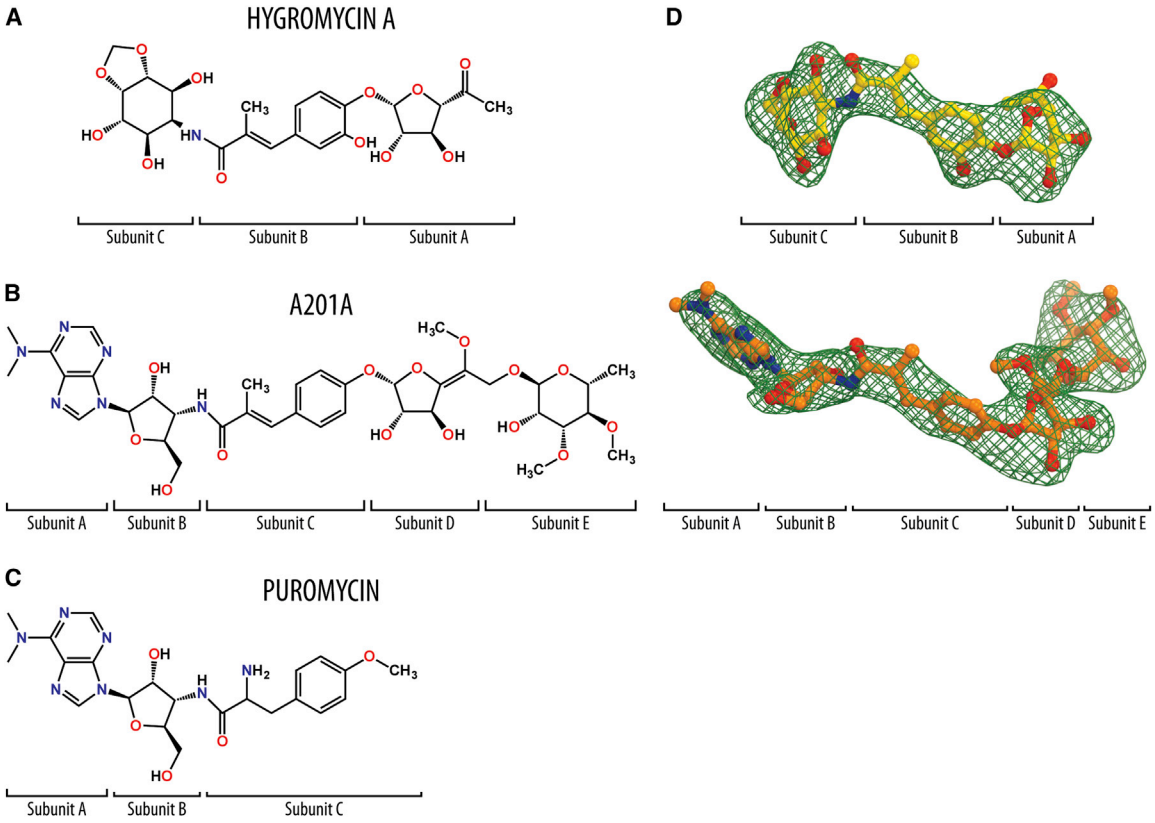

Figure 1. Chemical Structures and Electron Density Maps of Aminocyclitol Antibiotic HygA and Nucleoside Antibiotics A201A and PMN

(A–C) Chemical structures of (A) hygromycin A (HygA), (B) A201A, and (C) puromycin (PMN).

(D) Difference Fourier maps of HygA and A201A in complex with the *T. thermophilus* 70S ribosome (green mesh). The refined models of the drugs are displayed in their respective electron densities before refinement. The unbiased ($F_{obs} - F_{calc}$) difference electron density maps are contoured at 3.0σ. Carbon atoms are colored yellow for HygA and orange for A201A, nitrogens are blue, and oxygens are red.

(B), α-methyl-p-coumaric acid (C), an unnamed hexofuranose (D), and 3,4-di-O-methyl-D-rhamnose (E), connected linearly via one amide and three glycosidic linkages (Kirst et al., 1985). Subunits A–C of A201A are structurally similar to PMN, whereas subunits C and D of A201A are structurally similar to subunits A and B of HygA (Figures 1A–1C). A201A is active against Gram-positive aerobic and anaerobic bacteria and most Gram-negative anaerobic species (Epp and Allen, 1976). In contrast, it is weakly toxic to aerobic Gram-negative bacteria, certain fungi, and mammals (Ensminger and Wright, 1976). A201A has been reported to inhibit peptide bond formation on bacterial ribosomes (Epp and Allen, 1976), but it is less effective against eukaryotic ribosomes (Jiménez and Vázquez, 1983).

The total synthesis of HygA (Chida et al., 1989; Donohoe et al., 2009) and, more recently, A201A (Nie et al., 2014), as well as the ability to generate biosynthetic precursors with biological activity (Dhote et al., 2009; Habib et al., 2003; Palaniappan et al., 2006; Palaniappan et al., 2009), has further opened the way to developing successive generations of these antibiotics with improved antimicrobial properties. However, to fully understand the structure-activity relationships of HygA, A201A, and analogs thereof, insights into the molecular modes by which these antibiotics interact with the ribosome and inhibit translation are required.

Here we present X-ray crystal structures of HygA in complex with the *Thermus thermophilus* (*Tth*) vacant 70S ribosome as well as HygA and A201A in complex with *Tth* 70S ribosome bearing A-, P-, and E-site tRNAs, at resolutions ranging between 2.6–3.1 Å (Table 1). These structures reveal that HygA and A201A bind at a common site within the PTC, in a position overlapping with that of aminoacylated-A76 of an A-tRNA. The presence of HygA and A201A sterically blocks the accommodation of A-tRNA at the PTC, causing local distortions of the tRNA acceptor arm and CCA-end. Consistent with these observations, single-molecule Förster resonance energy transfer (smFRET) imaging revealed that HygA and A201A do not interfere with initial binding of the ternary complex but specifically slow the proofreading phase of A-tRNA selection by as much as 1,000-fold by preventing A-tRNA accommodation into the PTC.

RESULTS AND DISCUSSION

Structure of HygA in Complex with the 70S Ribosome

To determine the binding site of HygA on the ribosome, vacant *Tth* 70S ribosomes were crystallized in the presence of 100 μM HygA, and a structure of the complex was determined by X-ray crystallography at 3.1 Å resolution (Table 1). An

Table 1. Data Collection and Refinement Statistics

Crystals	70S-HygA	70S-HygA with A-, P- and E-tRNAs	70S-A201A with A-, P- and E-tRNAs
Diffraction data			
Space group	$P2_12_12_1$	$P2_12_12_1$	$P2_12_12_1$
Unit cell dimensions, Å (a × b × c)	209.51 × 448.29 × 619.37	208.39 × 444.58 × 619.20	208.89 × 446.22 × 619.48
Wavelength, Å	1.1000	0.9795	0.9795
Resolution range (outer shell), Å	310-3.10 (3.18-3.10)	361-2.60 (2.67-2.60)	262-2.65 (2.72-2.65)
I/σI (outer shell with I/σI = 1)	7.75 (1.01)	7.32 (1.04)	6.34 (1.03)
Resolution at which I/σI = 1, Å	3.10	2.60	2.65
Resolution at which I/σI = 2, Å	3.35	2.79	2.85
CC(1/2) at which I/σI = 1, %	26.8	19.0	27.2
Completeness (outer shell), %	99.9 (99.9)	99.3 (99.5)	98.5 (99.3)
R_{merge} (outer shell)%	22.7 (211.8)	18.6 (150.3)	15.0 (120.3)
No. of crystals used	1	1	1
No. of reflections used: observed	5,754,441	9,880,724	5,648,754
No. of reflections used: unique	1,041,680	1,725,274	1,628,435
Redundancy	5.52	5.73	3.47
Wilson B-factor, $Å^2$	81.2	51.7	50.7
Refinement			
R_{work}/R_{free}, %	23.2/28.3	23.3/28.3	22.6/27.1
No. of non-hydrogen atoms: RNA	192,347	200,165	200,193
No. of non-hydrogen atoms: protein	91,479	90,982	90,982
No. of non-hydrogen atoms: ions (Mg, K, Zn, Fe)	1,746	2,331	2,322
No. of non-hydrogen atoms: waters	2,922	3,530	3,713
Ramachandran plot: favored regions, %	95.52	93.39	93.04
Ramachandran plot: allowed regions, %	4.02	5.56	5.72
Ramachandran plot: outliers, %	0.45	1.06	1.24
Deviations from ideal values (RMSD): bond, Å	0.003	0.005	0.005
Deviations from ideal values (RMSD): angle, degrees	0.678	0.965	0.945
Deviations from ideal values (RMSD): chirality	0.031	0.041	0.040
Deviations from ideal values (RMSD): planarity	0.003	0.005	0.005
Deviations from ideal values (RMSD): dihedral, degrees	14.709	15.330	15.055
Deviations from ideal values (RMSD): average B-factor (overall), $Å^2$	82.3	58.2	59.0

$R_{merge} = \sum |I - \langle I \rangle| / \sum I$, where I is the observed intensity and $\langle I \rangle$ is the average intensity from multiple measurements.
$R_{work} = \sum |F_{obs} - F_{calc}| / \sum F_{obs}$. For calculation of R_{free}, 5% of the truncated data set was excluded from the refinement.

unbiased difference Fourier map, which was calculated using the observed amplitudes from the crystal and the amplitudes and phases derived from a model of the ribosome without the bound antibiotic, revealed positive density peaks resembling characteristic features of the HygA chemical structure (Figure 1D). A single binding site for HygA was observed on the ribosome within the PTC of the large ribosomal subunit (Figures 2A–2C).

In agreement with the ability of HygA to inhibit binding of PMN, aminoacylated tRNAs and tRNA fragments to the ribosomal A site (Guerrero and Modolell, 1980; Polacek et al., 2002; Poulsen et al., 2000), the binding site for HygA overlaps with the aminoacyl moiety and nucleotide A76 of an A-tRNA (Figure 2D). Unlike PMN, which contains an α-amino mimic on subunit C (Figure 1C), HygA has a methyl group in the equivalent position (Figure 1A) and therefore cannot act as an acceptor of the amino acid or nascent chain attached to the P-tRNA (Figure 2D). Thus, while PMN inhibits translation by promoting premature termination and release of the nascent polypeptide chain, HygA acts by sterically occluding the binding of A-site ligands.

Consistent with reports that HygA competes with chemically distinct PTC inhibitors for ribosome binding (Guerrero and Modolell, 1980), the binding site of HygA overlaps with those of chloramphenicol (Bulkley et al., 2010; Dunkle et al., 2010), linezolid (Ippolito et al., 2008; Wilson et al., 2008), and clindamycin (Dunkle et al., 2010; Schlünzen et al., 2001; Tu et al., 2005) (Figures S1A–S1D). The competition of HygA with 16-membered macrolide antibiotics, such as spiramycin, tylosin, or carbomycin, but not with 14-membered macrolides, such as erythromycin (ERY), is in accordance with the suggestion that the mycarose sugar moiety of the 16-membered macrolides (absent

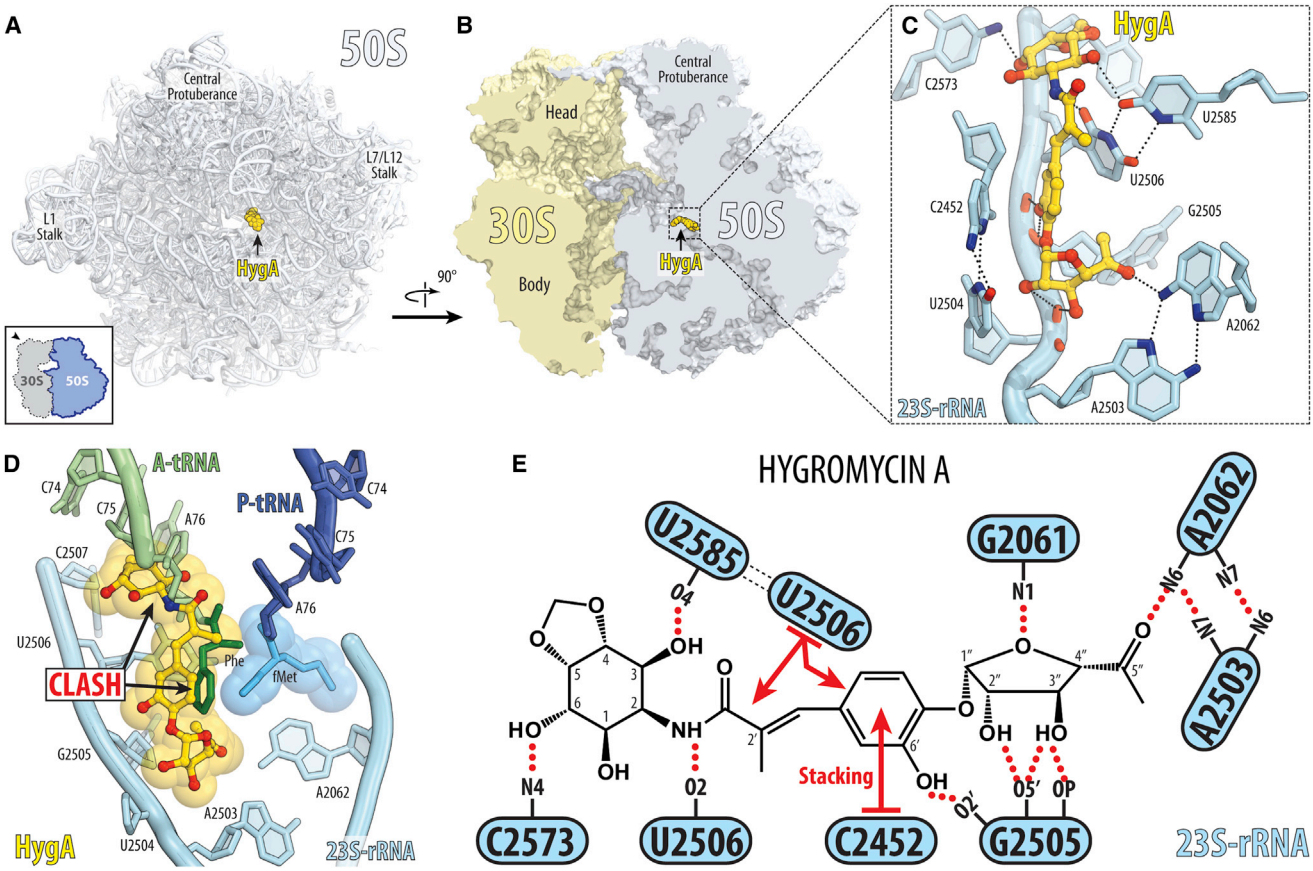

Figure 2. Structures of HygA on the Ribosome

(A and B) Overview of HygA binding sites on the 70S ribosome (30S, light yellow; 50S, light blue).

(C) Interactions of HygA (yellow) with 23S rRNA nucleotides (cyan) within the PTC.

(D) HygA (yellow) binding site relative to Phe-tRNA in the A site (green with Phe moiety colored dark green) and fMet-tRNA in the P site (dark blue with fMet moiety colored blue) (Polikanov et al., 2014b).

(E) Schematic representation of the interactions shown in (C). Potential H-bond interactions are indicated with dashed lines; stacking interactions are shown with red arrows. See also Figures S1 and S2.

in ERY) encroaches upon the HygA binding site (Poulsen et al., 2000) (Figures S2A–S2D).

Interactions of HygA at the PTC

HygA binds within the A-site cleft on the large ribosomal subunit with its aromatic subunit B sandwiched between U2506 and C2452 and is oriented such that the methylenedioxy ring of subunit C protrudes toward C2573, while the furanose ring of subunit A (at the other end of HygA) extends into the ribosome exit tunnel (Figures 2C and 2D). Binding of HygA appears to induce a rotation of U2506 toward the drug, compared to the position of U2506 in the *Tth* 70S lacking A- and P-tRNAs (Polikanov et al., 2012). In this position, U2506 forms base-pairing interactions with U2585, which explains protection of these bases from chemical modification in the presence of HygA (Poulsen et al., 2000).

HygA is highly hydrophilic, and its many hydroxyl groups establish numerous hydrogen bonding (H-bond) interactions with nucleotides of the 23S rRNA (Figures 2C and 2E). The C3 and C6 hydroxyls of the aminocyclitol ring of subunit C of HygA are within 3.1 Å and 2.7 Å from the O4 of U2585 and the N4 of C2573, respectively. These interactions are likely to be important, since HygA derivatives, where the C3 and C6 hydroxyls are methylated, exhibit reduced antimicrobial activity (Hecker et al., 1992). Although the methylenedioxy ring of subunit C of HygA has also been reported to be critical for biological activity (Chida et al., 1990; Hecker et al., 1992; Palaniappan et al., 2009), it does not appear to contribute directly to the interaction of HygA with the ribosome (Figure 2C). This observation agrees with the suggestion that the methylenedioxy ring is important to induce the twisted-boat conformation of the adjacent aminocyclitol ring (Chida et al., 1990; Hecker et al., 1992), which, in turn, orients the C3 and C6 hydroxyls to establish the observed H-bond interactions (Figures 2C and 2E). The C6′ hydroxyl in subunit B of HygA is within H-bond distance (2.9 Å) from the ribose 2′-OH of G2505. Substitutions of the C6′ hydroxyl generally lead to decreased antimicrobial activity (Hecker et al., 1993), highlighting the importance of HygA interaction with G2505. The hydroxyls of the furanose moiety of subunit A also potentially form H-bonds with A2062, U2504, and G2505 and

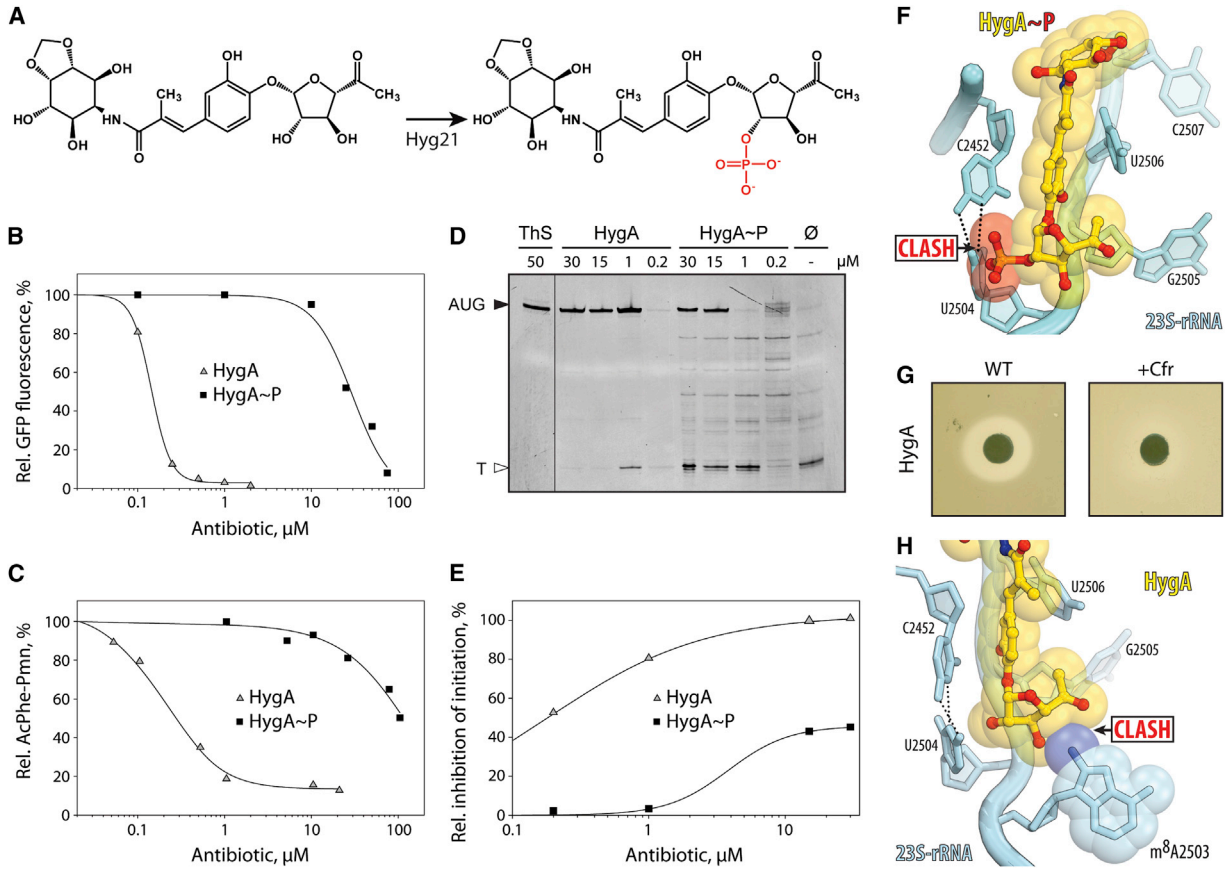

Figure 3. Resistance to HygA

(A) Schematic diagram illustrating the conversion of HygA to phosphorylated HygA (HygA∼P) catalyzed by Hyg21 O-phosphotransferase (Dhote et al., 2008).

(B) In vitro translation of green fluorescent protein (GFP) in the presence of increasing concentrations of HygA or HygA∼P.

(C) Puromycin reactivity of a ribosomal complex containing AcPhe-tRNA bound at the P site in the presence of increasing concentrations of HygA or HygA∼P.

(D) Toe-printing assay monitoring translation in the presence of increasing concentrations of HygA or HygA∼P. Additionally, control reactions without antibiotic (∅) or including thiostrepton (ThS) are shown. AUG designates location of the ribosomes stalled at the start codon; T denotes the position of the unique Thr codon, which stalls ribosomes because of the lack of Thr amino acid in the reaction mixture.

(E) Quantitation of (D) where the inhibition efficiency was calculated as a percentage of stalling at AUG relative to combined intensities of AUG and T.

(F) Molecular modeling of HygA∼P reveals a clash between the phosphate group and nucleobase of U2504 of the 23S rRNA.

(G) Disc-diffusion assay monitoring growth of wild-type *E. coli* strain lacking Cfr (WT, left) and the same strain expressing Cfr (+Cfr, right) in the presence of HygA (5 nmol).

(H) Molecular model of C8-methylation of A2503 by Cfr revealing a clash with the ribose of subunit A of HygA. See also Figure S3.

are thus likely to contribute to HygA binding affinity. Consistent with this notion, HygA analogs lacking the furanose ring (i.e., subunit BC compounds) are devoid of antimicrobial activity (Jaynes et al., 1993). The furanose sugar can, however, be substituted with simple lipophilic alkyl esters without loss of activity (Jaynes et al., 1992, 1993), indicating the possibility for development of better HygA derivatives via alterations within the subunit C region of the drug.

HygA Resistance Mechanisms

The strain of *S. hygroscopicus* that produces HygA is thought to obtain self-resistance to HygA using at least two mechanisms: (i) efflux of the drug by the putative proton-gradient-dependent efflux pumps Hyg19 and Hyg28 (Dhote et al., 2009) and (ii) inactivation of HygA through the action of the phosphotransferase Hyg21 (Dhote et al., 2008). The latter catalyzes the transfer of the γ-phosphoryl group from ATP to the ribose 2′-OH of subunit A of HygA (Figure 3A), rendering the drug inactive (Dhote et al., 2008). To ascertain whether the inactivity of phosphorylated HygA (HygA∼P) could be attributed to the abrogation of translation inhibition, rather than other factors such as decreased membrane penetration, we performed in vitro translation of GFP in the presence of increasing concentrations of HygA and HygA∼P (Figure 3B). Consistent with previous studies (Dhote et al., 2009; Guerrero and Modolell, 1980; Palaniappan et al., 2009), HygA displayed strong inhibitory properties, inhibiting GFP production with a half inhibitory concentration (IC_{50}) of 0.2 μM (Figure 3B). In contrast, HygA∼P was over 50-fold less effective, displaying an IC_{50} of 12 μM (Figure 3B). An even larger difference between HygA and HygA∼P was observed using the

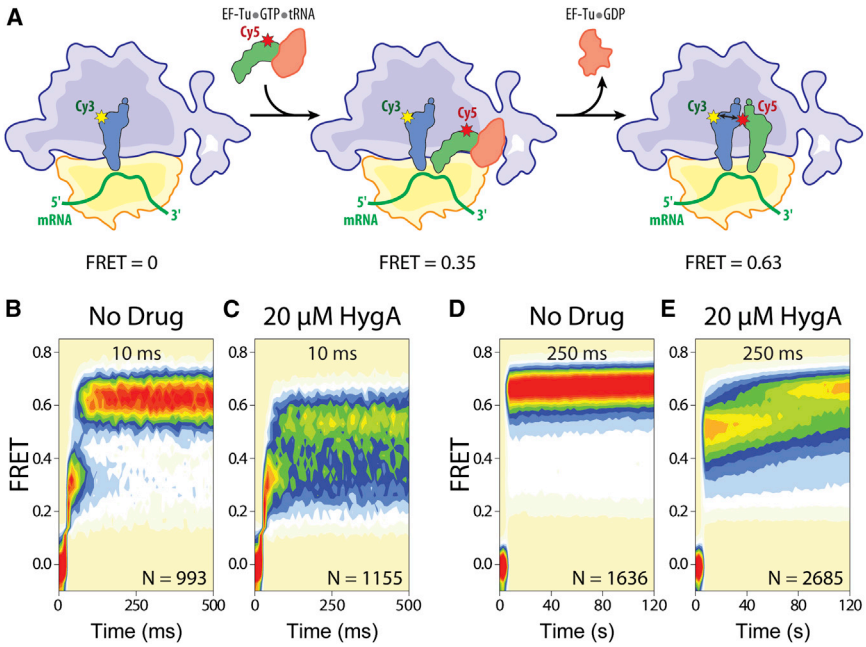

Figure 4. smFRET Analysis of the HygA Effect on tRNA Accommodation

(A) Schematic diagram illustrating the delivery of EF-Tu•GTP•tRNA ternary complex containing cognate Phe-tRNA^{Phe}(Cy5) to the A site of *E. coli* 70S ribosomes containing tRNA$_i^{Met}$(Cy3) in the P site, leading to intermediate (0.35) FRET during initial steps of codon recognition and high-FRET (0.63) upon A-site tRNA accommodation.

(B–E) Single-molecule FRET imaging of aa-tRNA selection performed under direct 532 nm excitation, using either a ([B] and [C]) 10 ms/frame or ([D] and [E]) 250 ms/frame time resolution in the absence of drugs ([B] and [D]), or with 20 μM HygA ([C] and [E]). The 2D histograms were generated by superimposing all individual FRET trajectories, aligned to the initial time point of non-zero FRET efficiency. See also Figure S4.

puromycin assay (Figure 3C), which monitors the formation of AcPhe-PMN when PMN is added to a ribosomal complex containing AcPhe-tRNA^{Phe} in the P site. The IC_{50} of HygA for the puromycin assay was 0.5 μM, whereas HygA∼P was 200 times less effective, exhibiting only 50% inhibition at 100 μM (Figure 3C). Toe-printing assays revealed that HygA stalls ribosomes at the mRNA start codon, whereas HygA∼P is much less effective as an inhibitor, allowing ribosomes to initiate and even enter the translation elongation stage (Figures 3D and 3E). Modeling the phosphate group onto the subunit A ribose 2′-OH showed a steric clash with U2504 of the 23S rRNA, providing a structural basis for the poor antimicrobial activity observed with HygA∼P (Fig. 3F).

Resistance to many peptidyl transferase inhibitors, such as chloramphenicol, lincomycin, and linezolid, is conferred by Cfr, a methyltransferase that monomethylates the C8 position of A2503 of the 23S rRNA (Long et al., 2006). To assess whether Cfr also confers resistance to HygA, we employed a disc-diffusion assay (Figure 3G). As expected, a ring of growth inhibition for the parental *E. coli* strain was observed around the origin where HygA was spotted onto the disc. In contrast, the growth inhibition was alleviated when the same strain contained a plasmid expressing Cfr, indicating acquired resistance to HygA (Figure 3G). Moreover, the toe-printing assay revealed that HygA is less effective as a translation initiation inhibitor when using Cfr-modified ribosomes (Figure S3A). Modeling the C8-methylation of A2503 shows a steric clash with the ribose of subunit A of HygA, providing a structural basis for the Cfr-mediated HygA resistance (Figure 3H).

HygA Allows Initial Binding but Prevents Full Accommodation of A-tRNA

To investigate the impact of HygA on the mechanism of aa-tRNA selection, we employed pre-steady-state smFRET imaging methods that enable real-time measurements of inter-tRNA distance during EF-Tu-catalyzed delivery of aa-tRNA to surface-immobilized ribosomes (Blanchard et al., 2004; Geggier et al., 2010). Here, the time evolution of FRET was monitored at a 10 ms/frame time resolution within individual 70S ribosomes bound with (Cy3-s^{4}U8) fMet-tRNA$_i^{Met}$ in the P site upon stopped-flow injection of ternary complex containing EF-Tu, GTP, and (Cy5-acp^{3}U47) Phe-tRNA^{Phe} (Figure 4A).

As expected from previous investigations in the absence of the drug (Geggier et al., 2010), productive FRET events leading to the incorporation of aa-tRNA at the A site evolved from a low- (∼0.2) to high-FRET (∼0.63) via the reversible transit of at least one intermediate-FRET (∼0.35) configuration (Figure 4B). The intermediate FRET value reflects the "A/T" state (Blanchard et al., 2004; Geggier et al., 2010), where ternary complex is bound within the ribosomal A site such that the tRNA anticodon is paired with mRNA in the small subunit and the acceptor stem interacts with EF-Tu (central panel in Figure 4A) (Schuette et al., 2009). Consistent with the rapid tRNA progression through the selection process, the time delay between the initial observation of low FRET and formation of the stable, high-FRET state, corresponding to the fully accommodated, classically configured (A/A) tRNA position (right panel in Figure 4A), was ∼60 ms.

In the presence of saturating concentrations of HygA (20 μM), aa-tRNA progression into the ribosome was strongly and specifically blocked at what appeared to be an intermediate state in the selection process that exhibited a FRET value (∼0.54) in between those of the GTPase-activated A/T (∼0.35 FRET) and fully accommodated (A/A) (∼0.63 FRET) positions (Figure 4C). By contrast, early steps in the selection process were unaffected, including the rate and efficiency with which this state was achieved (Figures 4C and S4A).

Notably, the inspection of fluorescence and FRET trajectories from single ribosomes revealed that the HygA-stalled ribosomes exhibited highly anti-correlated fluctuations in donor and acceptor intensities, reflecting rapid, reversible fluctuations

between intermediate- (~0.35) and high-FRET (~0.63) states (Figure S4B). Analogous fluctuations were also observed on drug-free ribosomes (Figure S4B) (Geggier et al., 2010), albeit for a much shorter period of time before stable accommodation. This important observation indicates that the FRET value observed at the population level (~0.54) for the stalled complex (Figure 4C) does not reflect a defined tRNA accommodation intermediate on the pathway between the A/T and A/A state, but rather a weighted average of the intermediate- and high-FRET states. The average high-FRET value observed in the presence of HygA (~0.54) resembled that for the inhibited fully-accommodated aa-tRNA (~0.63), indicating that HygA blocks a very late stage of aa-tRNA accommodation. Imaging experiments performed at a lower time resolution (250 ms/frame) indicated that the HygA-induced stall in tRNA selection persisted for ~60 s prior to complete accommodation of aa-tRNA at the PTC (Figures 4D, 4E, S4C, and S4D). At present, it is unclear whether EF-Tu remains bound to the ribosome during these processes.

Structure of 70S Complex with HygA and Bound A-Site tRNA

The observation from the FRET data that HygA and a partially accommodated tRNA-intermediate can co-exist on the ribosome suggested that it might be possible to investigate the structure of this state. To accomplish this, *Tth* 70S ribosomes containing mRNA and fMet-$tRNA_i^{Met}$ in the P site were co-crystallized with 100 μM HygA as well as with the cognate Phe-$tRNA^{Phe}$. The presence of A-, P-, and E-tRNAs significantly improved the X-ray diffraction quality compared to that of the vacant 70S ribosomes, enabling a structure of the complex to be determined at 2.6 Å resolution (Figure 5A; Table 1). In this complex, the binding site of HygA (Figures 5B and S5A; Movie S1) was identical to that observed in the absence of tRNAs (Figures 2C and 2E), with two main exceptions: (i) HygA appears to protect the P-tRNA from hydrolysis, leading to well-defined density for the fMet moiety of the P-site tRNA (Figure 5B) and (ii) the aminocyclitol ring of HygA establishes additional stacking interactions with the nucleobase of A76 of the A-tRNA (Figure 5C; Movie S1).

As expected, the presence of HygA precludes normal accommodation of A76 of A-tRNA within the PTC and causes A76 to adopt a previously unseen position, which is rotated by ~120° from its canonical position (Figure 5D; Movie S1). This rotated orientation of A76 induces a corresponding rotation in A2602, which thereby stacks upon the nucleobase of A76 (Figure 5D). The most dramatic consequences, however, are observed for nucleotides of the 3′ strand of the acceptor arm of the A-tRNA, which re-adjust their positions to account for the unaccommodated A76 position. This re-adjustment requires large-scale movements, including rotation of C74 and C75, as well as register shifts in the acceptor arm nucleotides that are propagated as far as G70 of the A-tRNA (Figure 5D).

A201A Prevents Full Accommodation of the A-Site tRNA

Since A201A and HygA are both peptidyl transferase inhibitors and share a number of related chemical features (Figures 1A and 1B), we employed the smFRET method to investigate whether A201A also interferes with the A-tRNA accommodation process (Figure 4). In the presence of saturating concentrations of A201A (20 μM), a delay was observed in the transition of the aa-tRNA into the high-FRET (~0.63) state (Figure 6A). As observed for HygA, fast, reversible fluctuations were observed between intermediate- and high-FRET states (Figure S4); however, the average FRET value exhibited by the A201A-stalled complex was ~0.56, modestly higher than that observed for HygA. Such dynamics persisted for ~5 s before completion of the selection process finally occurred (Figure 6B). This relatively modest delay in the selection process compared to that observed for HygA (Figure 4C) is consistent with its 10-fold increased IC_{50} (2 μM) for translation inhibition (Figure 6C).

Structure of A201A-70S Complex in the Presence of A-Site tRNA

To further investigate the interplay between A201A and the A-tRNA, we also determined a structure of A201A (100 μM) in complex with the *Tth* 70S ribosome with bound A- and P-tRNAs at 2.65 Å resolution (Figure 6D; Table 1). As expected, A201A binds in the A-site pocket of the PTC (Figure 6E; Movie S2), overlapping with the binding site of A-tRNA (Figure 6F). Specifically, the 6-N-dimethyl-3′-amino-3′-deoxyadenosyl moiety of A201A overlaps with the binding position of A76 of the A-tRNA (Figure 6F). Consistent with this observation, the toe-printing assay revealed that A201A, like HygA, causes stalling of the ribosomes at the start codon of mRNA, albeit less efficiently than HygA (Figure S3B). Similar to HygA, A201A has a methyl group on subunit C, where PMN contains the α-amino mimic and, therefore, A201A cannot act as a peptide-bond acceptor, as PMN does. The α-methyl-p-coumaric acid and the unsaturated furanose moieties of A201A, which are also present in HygA, make a similar network of H-bond interactions (Figures 6E and S5B), except that A201A lacks one hydroxyl group (that is present on subunit B of HygA; Figures 1A and 1B) and, therefore, cannot form the H-bonds with G2505 as observed for HygA (Figures 2C, 2E, and 5B). In addition to the efflux mechanism (Barrasa et al., 1995), self-resistance to A201A of *S. capreolus* NRRL 3817 is obtained via Ard2-mediated phosphorylation of the ribose 2′-OH of subunit D of A201A (Barrasa et al., 1997). Analogous to HygA, phosphorylation at this position could prevent drug binding by clashing with U2504 of the 23S rRNA. Moreover, disc-diffusion assays demonstrated that Cfr also confers resistance against A201A (Figure S3C).

Unlike HygA, A201A contains a unique 3,4-di-O-methyl-D-rhamnose moiety glycosidically linked to the furanose moiety, which extends deeper into the ribosomal tunnel and comes within H-bond distance of A2059 (Figure 6G). The position of the D-rhamnose moiety of A201A overlaps with the desosamine sugar of the macrolide ERY (Figure 6G; Movie S2), which also contacts A2059 (Bulkley et al., 2010; Dunkle et al., 2010; Schlünzen et al., 2001; Tu et al., 2005). Consistent with this observation, we could demonstrate that A201A competes with ERY for ribosome binding, whereas HygA (which lacks the D-rhamnose) does not (Figure 6H).

Because the nucleoside moiety of A201A occupies the position at the PTC that is normally taken by aminoacyl-A76 of the A-tRNA (Figure 6F), rearrangements of the acceptor arm of the A-tRNA are necessary to accommodate the binding of the

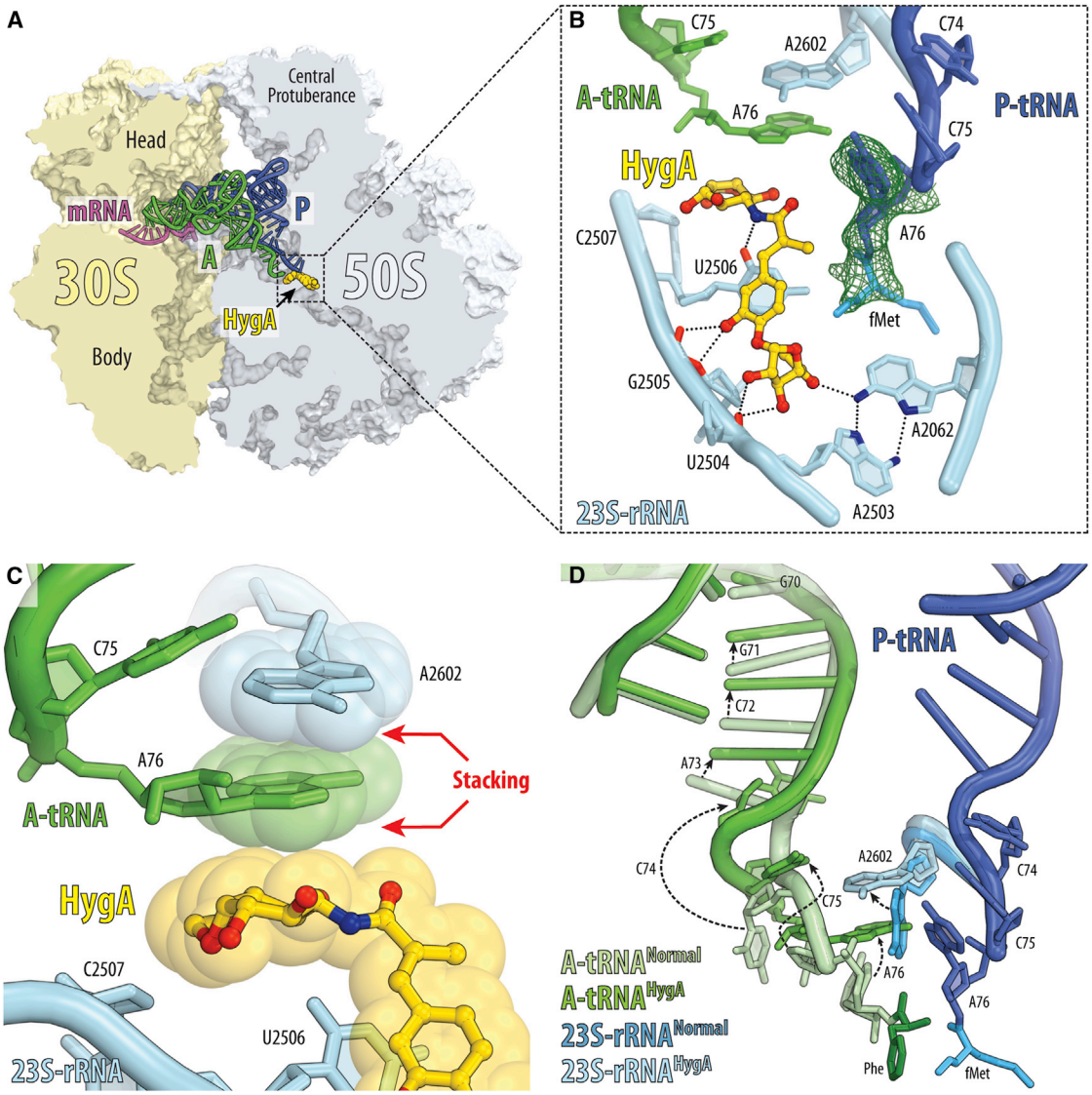

Figure 5. Structure of HygA-70S Ribosome Complex with A- and P-tRNAs

(A) Transverse section of 70S ribosome (30S, light yellow; 50S, light blue) showing HygA (yellow) relative to A-site tRNA (green), P-site tRNA (blue), and mRNA (magenta).

(B) Binding of HygA (yellow) to the ribosome prevents hydrolysis of the amino acid from the P-site tRNA, leading to clearly visible electron density for the fMet moiety (green mesh).

(C) Stacking interactions between A76 of A-tRNA (green), A2602 (cyan), and the aminocyclitol ring of HygA.

(D) Comparison of the position of A-tRNA in the presence of HygA (green, A-tRNA^{HygA}) with the canonical position of A-tRNA when fully accommodated in the A site (light green, A-tRNA^{Normal}). Relative positions of fMet-tRNA (blue) in the P site, and A2602 in the presence (cyan) and absence (blue) of HygA are also shown. See also Figures S5 and S7.

A-tRNA to the ribosome (Figure S6). The conformation of the A-tRNA CCA-end observed in the presence of A201A is distinct from that observed with HygA (Figure S6). While these rearrangements are reminiscent of those observed for P-tRNA in the presence of the antibiotic blasticidin S (Svidritskiy et al., 2013) and for deacylated tRNA bound at the E site (Schmeing et al., 2003; Selmer et al., 2006) (Figure S6), in these latter cases the conformational changes are local and do not disturb the overall conformation of the acceptor arm.

CONCLUSIONS

Collectively, our structural and biochemical results lead us to propose a model for the mechanism of translation inhibition by HygA and A201A (Figure 7). Both HygA and A201A allow binding of the initiator fMet-tRNA$_i^{Met}$ to the P site of the ribosome (Figures 7A and 7B). This is consistent with the toe-printing experiments showing that both HygA and A201A inhibit translation when the ribosome still resides at the start codon

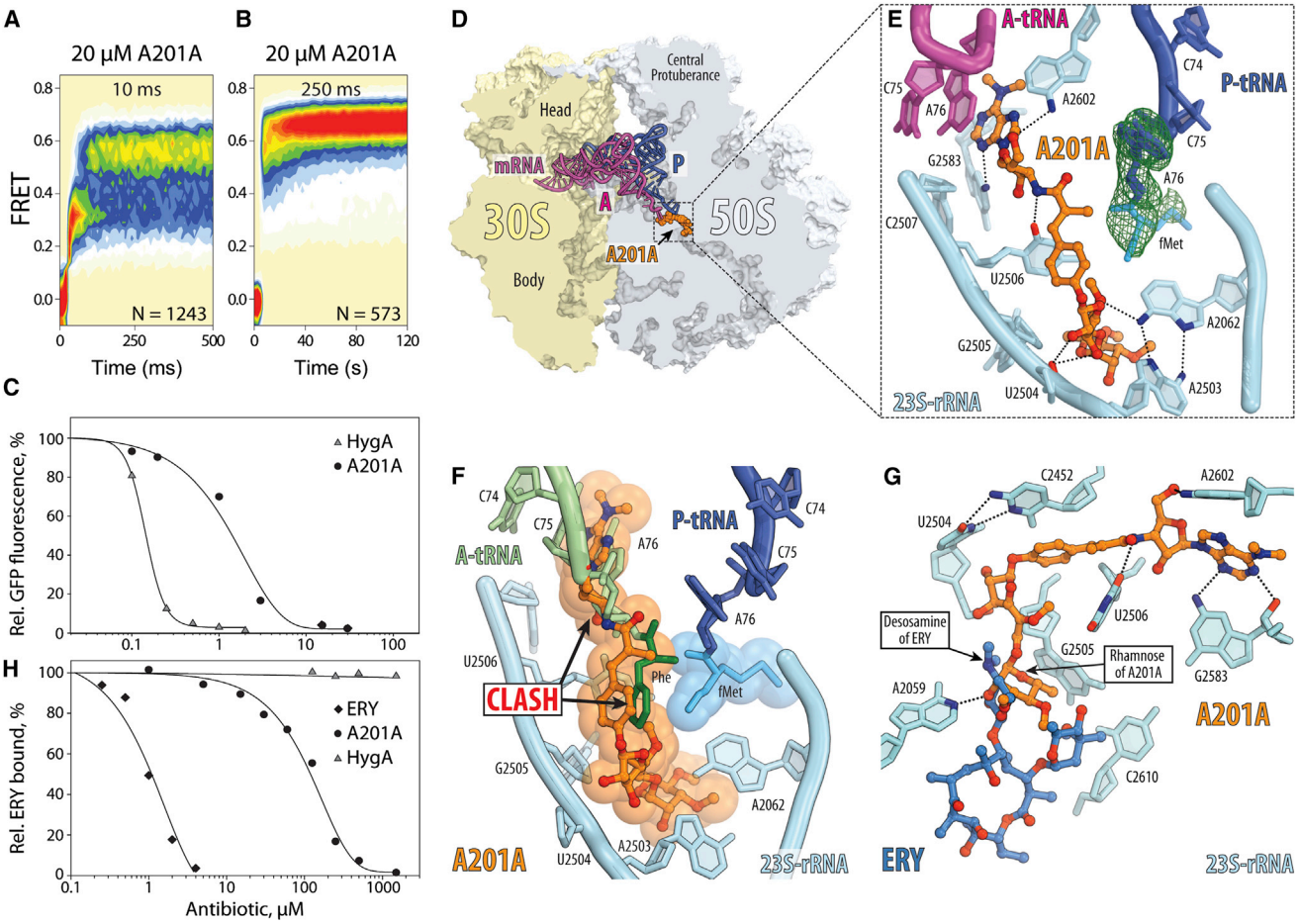

Figure 6. Effect of A201A on A-tRNA Accommodation Observed via smFRET and Structurally

(A and B) Single-molecule FRET imaging of aa-tRNA selection performed under direct 532 nm excitation, using either a (A) 10 ms/frame or (B) 250 ms/frame time resolution in the presence of 20 μM A201A.

(C) In vitro translation of GFP in the presence of increasing concentrations of HygA or A201A.

(D) Transverse section of 70S ribosome (30S, light yellow; 50S, light blue) showing the A201A (orange) relative to A-site tRNA (red), P-site tRNA (blue), and mRNA (magenta).

(E) Interactions of A201A (orange) with 23S rRNA nucleotides (cyan), A-tRNA (red), and fMet-tRNA (dark blue with fMet moiety colored light blue). Electron density for the fMet moiety is shown as a green mesh.

(F) A201A relative to Phe-tRNA in the A site (light green with Phe moiety colored dark green) (Polikanov et al., 2014b).

(G) Fucofuranose of A201A interacts with A2059 of the 23S rRNA and overlaps with the binding site of the desosamine sugar of ERY (blue).

(H) Competition assay showing binding of radiolabelled ERY to 70S ribosomes in the presence of increasing concentrations of HygA, A201A, or unlabeled ERY. Binding of radiolabeled ERY in the absence of other drugs is defined as 100%. See also Figures S3 and S5–S7.

(Figures 3D, 3E, and S3B). Structurally, we observe that the binding of either drug to the PTC leads to protection of the fMet-tRNA$_i^{Met}$ from hydrolysis (Figures 5B and 6E). However, we cannot rule out the possibility that HygA and A201A can also bind to post-translocational ribosomal complexes (that also have a free A site) and thus prevent translation during later elongation stages. Indeed, HygA has been shown to bind to ribosomes with Phe-tRNA^{Phe} in the P site (Guerrero and Modolell, 1980; Polacek et al., 2002; Poulsen et al., 2000) and also to promote binding of CACCA-AcLeu tRNA fragments to the ribosomal P site (Guerrero and Modolell, 1980), indicating that HygA binding and inhibition is not specific for P-site fMet-tRNA$_i^{Met}$, which was used in our studies.

Our smFRET experiments (Figure 4, 6A, and 6B) reveal that the delivery and initial binding of the EF-Tu-GTP- aa-tRNA ternary complex to the ribosomal A site remains unaffected by the presence of HygA or A201A (Figures 7B and 7C). In contrast, both drugs interfere with late steps in tRNA selection where the aa-tRNA rapidly transitions back and forth between A/T-like and accommodated positions (Figure 7D). These reversible FRET dynamics correspond to kinetic steps (k_4/k_{-4}) associated with tRNA movements between the GTPase-activated and accommodated states accompanying the proofreading phase of the selection process (Geggier et al., 2010; Whitford et al., 2010). Hence, these findings suggest that HygA specifically acts to sterically interfere with the productive

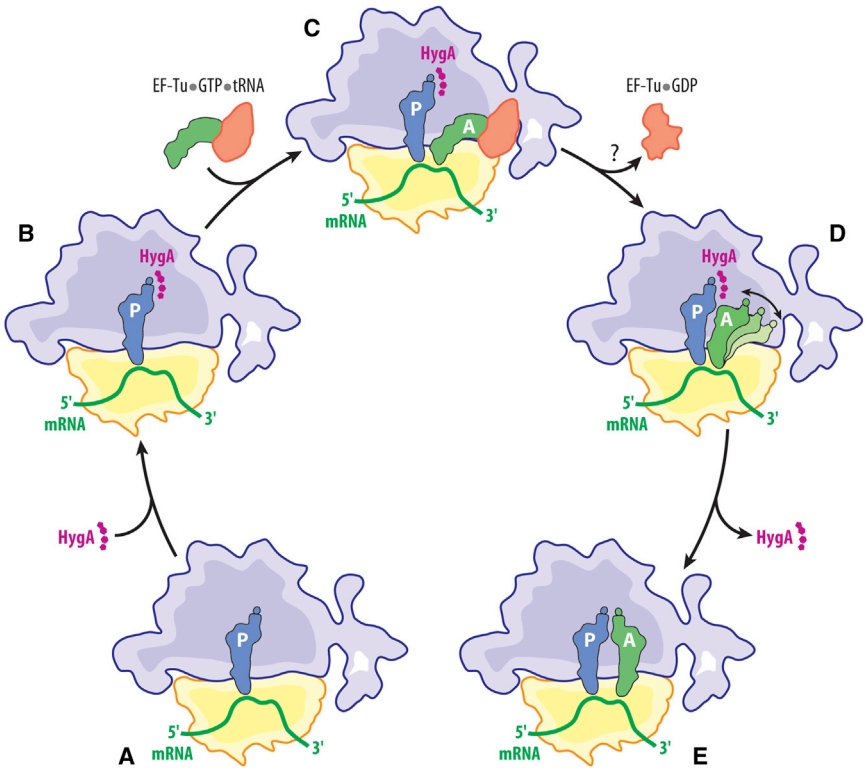

Figure 7. Model for Action of HygA and A201A during Translation

(A–E) Schematic diagram illustrating the mechanism of action of HygA and A201A to prevent full-accommodation of the A-tRNA during translation.

docking of the CCA end of the A-tRNA at the PTC upon successful navigation of the accommodation corridor (Sanbonmatsu et al., 2005; Whitford et al., 2010). Further experiments will be required to explore the relative timing of these A-tRNA movements with inorganic phosphate and EF-Tu release, which are also associated with proofreading, and to what extent HygA and A201A influence this process. The partially accommodated A-tRNA states observed in our X-ray structures in the presence of HygA or A201A have a fully-accommodated elbow region and therefore would be consistent with the high-FRET state observed in the smFRET experiments performed in the presence of the drugs (Figures 4A–4E, 6A, and 6B). However, we note that in both cases the tRNAs appeared to be deacylated, most likely due to the hydrolysis during crystallization. Nevertheless, in silico modeling the aminoacyl moiety back into the structures indicates that it would be possible to bind an aminoacylated tRNA in the partially accommodated states (Figure S7). Unlike the crystal structures in which only distinct partially accommodated states are observed, the smFRET experiments reveal that HygA and A201A cause the A-tRNA to oscillate between the A/T-like configuration and partially accommodated states for extended periods of time (5–60 s) (Movies S1 and S2). Stall durations of this magnitude (~100- to 1,000-fold longer than the uninhibited selection process of ~50 ms) are significant, especially when compared to the rate of translation (~10–20 aa/s) and may therefore explain why these drugs are effective translation inhibitors.

In conclusion, we have revealed the mode of interaction of the PTC inhibitors HygA and A201A with the ribosome, providing two scaffolds upon which to develop new improved antibiotics. Our studies uncovered the mechanism of action of HygA and A201A, both of which allow delivery and initial binding of the A-tRNA but prevent its full accommodation at the PTC. These data expand our knowledge of the mechanisms by which peptidyltransferase inhibitors impact tRNA selection and suggest the existence of functional states during proofreading that have yet to be identified.

EXPERIMENTAL PROCEDURES

Materials for Biochemical Experiments

Hygromycin A and derivatives were purified from wild-type or mutant *S. hygroscopicus* NRRL 2388 as described previously (Palaniappan et al., 2006). A201A was kindly provided by Dr. Antonio Jimenez. ERY and radiolabelled ERY were obtained from Sigma Aldrich and Perkin Elmer, respectively. Puromycin dihydrochloride and $tRNA^{Phe}$ were obtained from Sigma Aldrich; radiolabeled L-[2,3,4,5,6-^{3}H]phenylalanine was obtained from Amersham Biosciences. *E. coli* ribosomes and AcPhe-$tRNA^{Phe}$ were prepared as described previously (Blaha et al., 2000; Márquez et al., 2004). Cfr-modified ribosomes were prepared from an *E. coli* strain overexpressing Cfr. For crystallization, the 70S ribosomes from *Tth* and the unmodified $tRNA_i^{Met}$ and $tRNA^{Phe}$ from *E. coli* were purified and aminoacylated as previously described (Polikanov et al., 2014b), and the synthetic mRNA with the sequence 5′-GGC AAG GAG GUA AAA AUG UUC UAA-3′ was obtained from Integrated DNA Technologies.

In Vitro Translation and Binding Assays

The inhibition of GFP synthesis by HygA, HygA~P, or A201A was assessed using *E. coli* lysate-based transcription-translation-coupled assay (RTS100, 5Prime) and as described previously (Starosta et al., 2009, 2010). The peptidyl transferase activity in the presence or absence of antibiotic was measured using the puromycin reaction as described previously (Mamos et al., 2013). Binding of HygA, A201A, and ERY to an empty *E. coli* ribosome was monitored using a competition assay with radiolabelled [^{14}C]- ERY (170 dpm/pmol) as described before (Karahalios et al., 2006; Petropoulos et al., 2009; Starosta et al., 2010). The position of the ribosome on the mRNA was monitored using a toe-printing assay based on the in-vitro-coupled transcription-translation system using the PURExpress Δaa ΔtRNA kit (New England Biolabs) as described previously (Starosta et al., 2014). Further details on the in vitro translation and binding assays are provided in the Supplemental Experimental Procedures

Disc-Diffusion Assay

Disc-diffusion assays were performed as described by (Bailey et al., 2008). Briefly, the *E. coli* strain SQ110DTC (Δ*tolC*), which is hyper-sensitive to antibiotics (Orelle et al., 2013), was transformed with the plasmid pBgIII expressing Cfr (Kehrenberg et al., 2005), or the parental plasmid pBluescript II SK+ (Stratagen) and was plated onto LB plates. A 5-mm diameter sterile Whatmann 3MM paper disc spotted with 10 μl of 500 μM HygA (or A201A) was placed in the center of the plate, which was then incubated overnight at 37°C. Antibiotic resistance was measured by monitoring the ring of growth inhibition around the antibiotic-containing disc.

Single-Molecule FRET Imaging

The smFRET experiments were performed as described previously (Blanchard et al., 2004; Munro et al., 2007) and are described in detail in the Supplemental Experimental Procedures. To increase the FRET imaging duration and overall signal-to-noise ratio of imaging, an intra-molecularly photostabilized derivative of Cy5 was employed in combination with a cocktail of solution-protective agents (Juette et al., 2014; Zheng et al., 2014). To minimize the contribution of hybrid state tRNA configurations formed after peptide bond formation, experiments were performed using complexes lacking ribosomal protein L1 (Munro et al., 2007). Fluorescence and FRET traces were selected for analysis using semi-automated smFRET analysis software implemented in Matlab (The MathWorks) as previously described (Geggier et al., 2010).

Crystallographic Structure Determination

For details of structure determination refer to the Supplemental Experimental Procedures. Briefly, ribosome complexes with mRNA and tRNAs were formed essentially as described previously (Polikanov et al., 2014a; Voorhees et al., 2009). In the co-crystallization experiments with either HygA or A201A, the antibiotic was added to a final concentration of 100 μM. Crystals were grown by the vapor diffusion method in sitting drops at 19°C and stabilized as described previously (Polikanov et al., 2012, 2014a) with the antibiotics included in the stabilization buffers (100 μM HygA or 100 μM A201A). Each structure was solved and refined as described previously (Polikanov et al., 2014a; Adams et al., 2010; Emsley and Cowtan, 2004; McCoy et al., 2007). The statistics of data collection and refinement for each complex are compiled in Table 1.

ACCESSION NUMBERS

Coordinates and structure factors were deposited in the RCSB Protein Data Bank with accession codes 4Z3R for the *Tth* 70S ribosome in complex with HygA; 4Z3Q for the *Tth* 70S ribosome with HygA, A-, P- and E-site tRNAs, and 4Z3S for the *Tth* 70S ribosome in complex with A201A, A-, P-, and E-site tRNAs.

SUPPLEMENTAL INFORMATION

Supplemental Information includes seven figures, two movies, and Supplemental Experimental Procedures and can be found with this article online at http://dx.doi.org/10.1016/j.molcel.2015.04.014.

AUTHOR CONTRIBUTIONS

Y.S.P. designed and performed X-ray crystallography experiments. A.L.S. performed toe-printing, in vitro translation, binding, and disc-diffusion assays. M.F.J., R.B.A., D.S.T., B.J.B., and S.C.B. designed and performed smFRET experiments. W.L. and K.A.R. isolated and purified HygA. All authors interpreted data. Y.S.P., S.C.B., T.A.S., and D.N.W. wrote the manuscript.

ACKNOWLEDGMENTS

We thank Dr. A. Jimenez for kindly providing A201A compound, Dr. B. Vester for the Cfr-expressing plasmid, Dr. A.S. Mankin for providing the SQ110DTC strain, M. Stavropoulou and U. Antczak for technical help, and R.L. Grodzicki for preparation of the unmodified tRNAs (for structural studies). We also thank the staff at the Advanced Photon Source (beamline 24ID), supported by award GM103403 from the National Center for Research Resources at the National Institutes of Health; the staff at the National Synchrotron Light Source (beamline X25) for help during data collection; and the staff at the Richards Center at Yale University for computational support. This research was supported by grants from the National Institutes of Health (GM022778 to T.A.S., GM095737 to K.A.R. and D.N.W., and GM079238 and GM098859 to S.C.B.), HFSP (to D.N.W and S.C.B), the Deutsche Forschungsgemeinschaft (FOR1805, WI3285/3-1 and GRK1721 to D.N.W.), and the German Academic Exchange Service (DAAD postdoctoral fellowship to M.F.J.).

Received: January 5, 2015
Revised: February 23, 2015
Accepted: April 7, 2015
Published: May 28, 2015

REFERENCES

Adams, P.D., Afonine, P.V., Bunkóczi, G., Chen, V.B., Davis, I.W., Echols, N., Headd, J.J., Hung, L.W., Kapral, G.J., Grosse-Kunstleve, R.W., et al. (2010). PHENIX: a comprehensive Python-based system for macromolecular structure solution. Acta Crystallogr. D Biol. Crystallogr. *66*, 213–221.

Bailey, M., Chettiath, T., and Mankin, A.S. (2008). Induction of erm(C) expression by noninducing antibiotics. Antimicrob. Agents Chemother. *52*, 866–874.

Barrasa, M.I., Tercero, J.A., Lacalle, R.A., and Jimenez, A. (1995). The ard1 gene from *Streptomyces capreolus* encodes a polypeptide of the ABC-transporters superfamily which confers resistance to the aminonucleoside antibiotic A201A. Eur. J. Biochem. *228*, 562–569.

Barrasa, M.I., Tercero, J.A., and Jimenez, A. (1997). The aminonucleoside antibiotic A201A is inactivated by a phosphotransferase activity from *Streptomyces capreolus* NRRL 3817, the producing organism. Isolation and molecular characterization of the relevant encoding gene and its DNA flanking regions. Eur. J. Biochem. *245*, 54–63.

Blaha, G., Stelzl, U., Spahn, C.M., Agrawal, R.K., Frank, J., and Nierhaus, K.H. (2000). Preparation of functional ribosomal complexes and effect of buffer conditions on tRNA positions observed by cryoelectron microscopy. Methods Enzymol. *317*, 292–309.

Blanchard, S.C., Gonzalez, R.L., Kim, H.D., Chu, S., and Puglisi, J.D. (2004). tRNA selection and kinetic proofreading in translation. Nat. Struct. Mol. Biol. *11*, 1008–1014.

Bulkley, D., Innis, C.A., Blaha, G., and Steitz, T.A. (2010). Revisiting the structures of several antibiotics bound to the bacterial ribosome. Proc. Natl. Acad. Sci. USA *107*, 17158–17163.

Chida, N., Ohtsuka, M., Nakazawa, K., and Ogawa, S. (1989). Total synthesis of hygromycin A. J. Chem. Soc. Chem. Comm. 436–438.

Chida, N., Nakazawa, K., Ohtsuka, M., Suzuki, M., and Ogawa, S. (1990). Total synthesis of methoxyhygromycin and its 5-epimer. Chem. Lett. 423–426.

Dhote, V., Gupta, S., and Reynolds, K.A. (2008). An O-phosphotransferase catalyzes phosphorylation of hygromycin A in the antibiotic-producing organism *Streptomyces hygroscopicus*. Antimicrob. Agents Chemother. *52*, 3580–3588.

Dhote, V., Starosta, A.L., Wilson, D.N., and Reynolds, K.A. (2009). The final step of hygromycin A biosynthesis, oxidation of C-5″-dihydrohygromycin A, is linked to a putative proton gradient-dependent efflux. Antimicrob. Agents Chemother. *53*, 5163–5172.

Donohoe, T.J., Flores, A., Bataille, C.J., and Churruca, F. (2009). Synthesis of (-)-hygromycin A: application of Mitsunobu glycosylation and tethered aminohydroxylation. Angew. Chem. Int. Ed. Engl. *48*, 6507–6510.

Dunkle, J.A., Xiong, L., Mankin, A.S., and Cate, J.H. (2010). Structures of the *Escherichia coli* ribosome with antibiotics bound near the peptidyl transferase center explain spectra of drug action. Proc. Natl. Acad. Sci. USA *107*, 17152–17157.

Emsley, P., and Cowtan, K. (2004). Coot: model-building tools for molecular graphics. Acta Crystallogr. D Biol. Crystallogr. *60*, 2126–2132.

Ensminger, P.W., and Wright, W.E. (1976). A201A, a new antibiotic produced by *Streptomnyces cupreolus*. II. Biological studies. In 16th Intersci. Conf Antimicrob (Chicago: Agents Chemother).

Epp, J.K., and Allen, N.E. (1976). A201A, a new antibiotic produced by *Streptomyces capreolus*, IV. Mode of action studies. In 16th Intersci. Con$ Antimicrob (Chicago: Agents Chemothel), p. 63.

Geggier, P., Dave, R., Feldman, M.B., Terry, D.S., Altman, R.B., Munro, J.B., and Blanchard, S.C. (2010). Conformational sampling of aminoacyl-tRNA during selection on the bacterial ribosome. J. Mol. Biol. *399*, 576–595.

Guerrero, M.D., and Modolell, J. (1980). Hygromycin A, a novel inhibitor of ribosomal peptidyltransferase. Eur. J. Biochem. *107*, 409–414.

Habib, S.E., Scarsdale, J.N., and Reynolds, K.A. (2003). Biosynthetic origin of hygromycin A. Antimicrob. Agents Chemother. *47*, 2065–2071.

Hayashi, S.F., Norcia, L.J.L., Seibel, S.B., and Silvia, A.M. (1997). Structure-activity relationships of hygromycin A and its analogs: protein synthesis inhibition activity in a cell free system. J. Antibiot. *50*, 514–521.

Hecker, S.J., Lilley, S.C., and Werner, K.M. (1992). Hygromycin A - preparation of aminocyclitol analogs defining the minimum functionality required for biological activity. Bioorg. Med. Chem. Lett. *2*, 1043–1046.

Hecker, S.J., Lilley, S.C., Minich, M.L., and Werner, K.M. (1993). Application of hygromycin A structure-activity relationships to the antibiotic A201A. Bioorg. Med. Chem. Lett. *3*, 295–298.

Ippolito, J.A., Kanyo, Z.F., Wang, D., Franceschi, F.J., Moore, P.B., Steitz, T.A., and Duffy, E.M. (2008). Crystal structure of the oxazolidinone antibiotic linezolid bound to the 50S ribosomal subunit. J. Med. Chem. *51*, 3353–3356.

Jaynes, B.H., Elliott, N.C., and Schicho, D.L. (1992). Semisynthetic hygromycin A analogs: synthesis and anti-bacterial activity of derivatives lacking the furanose moiety. J. Antibiot. *45*, 1705–1707.

Jaynes, B.H., Cooper, C.B., Hecker, S.J., Blair, K.T., Elliott, N.C., Lilley, S.C., Minich, M.L., Schicho, D.L., and Werner, K.M. (1993). Synthesis and in vitro antibacterial activity of hygromycin A analogs modified at the C4' aryl position. Bioorg. Med. Chem. Lett. *3*, 1531–1536.

Jiménez, A., and Vázquez, D. (1983). Novel inhibitors of translation in eukaryotic systems. In Modes and mechanisms of microbial growth inhibitors. Antibiotics, F.E. Hahn, ed. (Berlin: Springer-Verlag), pp. 248–254.

Juette, M.F., Terry, D.S., Wasserman, M.R., Zhou, Z., Altman, R.B., Zheng, Q., and Blanchard, S.C. (2014). The bright future of single-molecule fluorescence imaging. Curr. Opin. Chem. Biol. *20*, 103–111.

Kakinuma, K., Kitahara, S., Watanabe, K., Sakagami, Y., Fukuyasu, T., Shimura, M., Ueda, M., and Sekizawa, Y. (1976). On the structure of hygromycin. The location of a methylene substituent and the anomeric configuration of the arabino-hexoside moiety. J. Antibiot. *29*, 771–773.

Karahalios, P., Kalpaxis, D.L., Fu, H., Katz, L., Wilson, D.N., and Dinos, G.P. (2006). On the mechanism of action of 9-O-arylalkyloxime derivatives of 6-O-mycaminosyltylonolide, a new class of 16-membered macrolide antibiotics. Mol. Pharmacol. *70*, 1271–1280.

Kehrenberg, C., Schwarz, S., Jacobsen, L., Hansen, L.H., and Vester, B. (2005). A new mechanism for chloramphenicol, florfenicol and clindamycin resistance: methylation of 23S ribosomal RNA at A2503. Mol. Microbiol. *57*, 1064–1073.

Kim, S.D., Kweon, M.H., Kim, C.J., and Yoo, I.D. (1990). Hygromycin, a plant growth inhibitor. Korean J. Biochem. 23.

Kirst, H.A., Dorman, D.E., Occolowitz, J.L., Jones, N.D., Paschal, J.W., Hamill, R.L., and Szymanski, E.F. (1985). The structure of A201A, a novel nucleoside antibiotic. J. Antibiot. *38*, 575–586.

Lee, H.B., Kim, C.J., Kim, J.S., Hong, K.S., and Cho, K.Y. (2003). A bleaching herbicidal activity of methoxyhygromycin (MHM) produced by an actinomycete strain *Streptomyces sp.* 8E-12. Lett. Appl. Microbiol. *36*, 387–391.

Long, K.S., Poehlsgaard, J., Kehrenberg, C., Schwarz, S., and Vester, B. (2006). The Cfr rRNA methyltransferase confers resistance to Phenicols, Lincosamides, Oxazolidinones, Pleuromutilins, and Streptogramin A antibiotics. Antimicrob. Agents Chemother. *50*, 2500–2505.

Mamos, P.L., Krokidis, M.G., Papadas, A.T., Karahalios, P., Starosta, A.L., Wilson, D.N., Kalpaxis, D.L., and Dinos, G.P. (2013). On the use of the antibiotic chloramphenicol to target polypeptide chain mimics to the ribosomal exit tunnel. Biochimie *95*, 1765–1772.

Mann, R.L., and Bromer, W.W. (1958). The isolation of a 2nd antibiotic from *Streptomyces hygroscopicus*. J. Am. Chem. Soc. *80*, 2714–2716.

Mann, R.L., and Woolf, D.O. (1957). Hygromycin. III. Structure studies. J. Am. Chem. Soc. *79*, 120–126.

Mann, R.L., Gale, R.M., and Van Abeele, F.R. (1953). Hygromycin. II. Isolation and properties. Antibiot Chemother (Northfield) *3*, 1279–1282.

Márquez, V., Wilson, D.N., Tate, W.P., Triana-Alonso, F., and Nierhaus, K.H. (2004). Maintaining the ribosomal reading frame: the influence of the E site during translational regulation of release factor 2. Cell *118*, 45–55.

McCoy, A.J., Grosse-Kunstleve, R.W., Adams, P.D., Winn, M.D., Storoni, L.C., and Read, R.J. (2007). Phaser crystallographic software. J. Appl. Cryst. *40*, 658–674.

Munro, J.B., Altman, R.B., O'Connor, N., and Blanchard, S.C. (2007). Identification of two distinct hybrid state intermediates on the ribosome. Mol. Cell *25*, 505–517.

Nakagawa, A., Fujimoto, T., Omura, S., Walsh, J.C., Stotish, R.L., and George, B. (1987). Hygromycin A, an antitreponemal substance. II. Therapeutic effect for swine dysentery. J. Antibiot. *40*, 1627–1635.

Nie, S., Li, W., and Yu, B. (2014). Total synthesis of nucleoside antibiotic A201A. J. Am. Chem. Soc. *136*, 4157–4160.

Omura, S., Nakagawa, A., Fujimoto, T., Saito, K., Otoguro, K., and Walsh, J.C. (1987). Hygromycin A, an antitreponemal substance. I. Screening method and therapeutic effect for *Treponema hyodysenteriae*-caused infection in CF-1 mice. J. Antibiot. *40*, 1619–1626.

Orelle, C., Carlson, S., Kaushal, B., Almutairi, M.M., Liu, H., Ochabowicz, A., Quan, S., Pham, V.C., Squires, C.L., Murphy, B.T., and Mankin, A.S. (2013). Tools for characterizing bacterial protein synthesis inhibitors. Antimicrob. Agents Chemother. *57*, 5994–6004.

Palaniappan, N., Ayers, S., Gupta, S., Habib, S., and Reynolds, K.A. (2006). Production of hygromycin A analogs in *Streptomyces hygroscopicus* NRRL 2388 through identification and manipulation of the biosynthetic gene cluster. Chem. Biol. *13*, 753–764.

Palaniappan, N., Dhote, V., Ayers, S., Starosta, A.L., Wilson, D.N., and Reynolds, K.A. (2009). Biosynthesis of the aminocyclitol subunit of hygromycin A in *Streptomyces hygroscopicus* NRRL 2388. Chem. Biol. *16*, 1180–1189.

Petropoulos, A.D., Kouvela, E.C., Starosta, A.L., Wilson, D.N., Dinos, G.P., and Kalpaxis, D.L. (2009). Time-resolved binding of azithromycin to *Escherichia coli* ribosomes. J. Mol. Biol. *385*, 1179–1192.

Pittenger, R.C., Wolfe, R.N., Hoehn, M.M., Marks, P.N., Daily, W.A., and McGUIRE, J.M. (1953). Hygromycin. I. Preliminary studies on the production and biologic activity of a new antibiotic. Antibiot Chemother (Northfield) *3*, 1268–1278.

Polacek, N., Swaney, S., Shinabarger, D., and Mankin, A.S. (2002). SPARK—a novel method to monitor ribosomal peptidyl transferase activity. Biochemistry *41*, 11602–11610.

Polikanov, Y.S., Blaha, G.M., and Steitz, T.A. (2012). How hibernation factors RMF, HPF, and YfiA turn off protein synthesis. Science *336*, 915–918.

Polikanov, Y.S., Osterman, I.A., Szal, T., Tashlitsky, V.N., Serebryakova, M.V., Kusochek, P., Bulkley, D., Malanicheva, I.A., Efimenko, T.A., Efremenkova, O.V., et al. (2014a). Amicoumacin a inhibits translation by stabilizing mRNA interaction with the ribosome. Mol. Cell *56*, 531–540.

Polikanov, Y.S., Steitz, T.A., and Innis, C.A. (2014b). A proton wire to couple aminoacyl-tRNA accommodation and peptide-bond formation on the ribosome. Nat. Struct. Mol. Biol. *21*, 787–793.

Poulsen, S.M., Kofoed, C., and Vester, B. (2000). Inhibition of the ribosomal peptidyl transferase reaction by the mycarose moiety of the antibiotics carbomycin, spiramycin and tylosin. J. Mol. Biol. *304*, 471–481.

Sanbonmatsu, K.Y., Joseph, S., and Tung, C.S. (2005). Simulating movement of tRNA into the ribosome during decoding. Proc. Natl. Acad. Sci. USA *102*, 15854–15859.

Schlünzen, F., Zarivach, R., Harms, J., Bashan, A., Tocilj, A., Albrecht, R., Yonath, A., and Franceschi, F. (2001). Structural basis for the interaction of antibiotics with the peptidyl transferase centre in eubacteria. Nature *413*, 814–821.

Schmeing, T.M., Moore, P.B., and Steitz, T.A. (2003). Structures of deacylated tRNA mimics bound to the E site of the large ribosomal subunit. RNA *9*, 1345–1352.

Schuette, J.C., Murphy, F.V., 4th, Kelley, A.C., Weir, J.R., Giesebrecht, J., Connell, S.R., Loerke, J., Mielke, T., Zhang, W., Penczek, P.A., et al. (2009). GTPase activation of elongation factor EF-Tu by the ribosome during decoding. EMBO J. *28*, 755–765.

Selmer, M., Dunham, C.M., Murphy, F.V., 4th, Weixlbaumer, A., Petry, S., Kelley, A.C., Weir, J.R., and Ramakrishnan, V. (2006). Structure of the 70S ribosome complexed with mRNA and tRNA. Science *313*, 1935–1942.

Starosta, A.L., Qin, H., Mikolajka, A., Leung, G.Y., Schwinghammer, K., Nicolaou, K.C., Chen, D.Y., Cooperman, B.S., and Wilson, D.N. (2009). Identification of distinct thiopeptide-antibiotic precursor lead compounds using translation machinery assays. Chem. Biol. *16*, 1087–1096.

Starosta, A.L., Karpenko, V.V., Shishkina, A.V., Mikolajka, A., Sumbatyan, N.V., Schluenzen, F., Korshunova, G.A., Bogdanov, A.A., and Wilson, D.N. (2010). Interplay between the ribosomal tunnel, nascent chain, and macrolides influences drug inhibition. Chem. Biol. *17*, 504–514.

Starosta, A.L., Lassak, J., Peil, L., Atkinson, G.C., Virumäe, K., Tenson, T., Remme, J., Jung, K., and Wilson, D.N. (2014). Translational stalling at polyproline stretches is modulated by the sequence context upstream of the stall site. Nucleic Acids Res. *42*, 10711–10719.

Sutcliffe, J.A. (2011). Antibiotics in development targeting protein synthesis. Ann. N Y Acad. Sci. *1241*, 122–152.

Svidritskiy, E., Ling, C., Ermolenko, D.N., and Korostelev, A.A. (2013). Blasticidin S inhibits translation by trapping deformed tRNA on the ribosome. Proc. Natl. Acad. Sci. USA *110*, 12283–12288.

Tu, D., Blaha, G., Moore, P.B., and Steitz, T.A. (2005). Structures of MLSBK antibiotics bound to mutated large ribosomal subunits provide a structural explanation for resistance. Cell *121*, 257–270.

Uyeda, M., Mizukami, M., Yokomizo, K., and Suzuki, K. (2001). Pentalenolactone I and hygromycin A, immunosuppressants produced by *Streptomyces filipinensis* and *Streptomyces hygroscopicus*. Biosci. Biotechnol. Biochem. *65*, 1252–1254.

Voorhees, R.M., Weixlbaumer, A., Loakes, D., Kelley, A.C., and Ramakrishnan, V. (2009). Insights into substrate stabilization from snapshots of the peptidyl transferase center of the intact 70S ribosome. Nat. Struct. Mol. Biol. *16*, 528–533.

Wakisaka, Y., Koizumi, K., Nishimoto, Y., Kobayashi, M., and Tsuji, N. (1980). Hygromycin and epihygromycin from a bacterium, *Corynebacterium equi* No. 2841. J. Antibiot. *33*, 695–704.

Whitford, P.C., Geggier, P., Altman, R.B., Blanchard, S.C., Onuchic, J.N., and Sanbonmatsu, K.Y. (2010). Accommodation of aminoacyl-tRNA into the ribosome involves reversible excursions along multiple pathways. RNA *16*, 1196–1204.

Wilson, D.N. (2009). The A-Z of bacterial translation inhibitors. Crit. Rev. Biochem. Mol. Biol. *44*, 393–433.

Wilson, D.N. (2014). Ribosome-targeting antibiotics and bacterial resistance mechanisms. Nat. Rev. Microbiol. *12*, 35–48.

Wilson, D.N., Schluenzen, F., Harms, J.M., Starosta, A.L., Connell, S.R., and Fucini, P. (2008). The oxazolidinone antibiotics perturb the ribosomal peptidyl-transferase center and effect tRNA positioning. Proc. Natl. Acad. Sci. USA *105*, 13339–13344.

Yoshida, M., Takahashi, E., Uozumi, T., and Beppu, T. (1986). Hygromycin A and methoxyhygromycin, novel inhibitors of K88-antigen synthesis of enterotoxic *Escherichia coli* strain. Agric. Biol. Chem. Tokyo *50*, 143–149.

Zheng, Q., Juette, M.F., Jockusch, S., Wasserman, M.R., Zhou, Z., Altman, R.B., and Blanchard, S.C. (2014). Ultra-stable organic fluorophores for single-molecule research. Chem. Soc. Rev. *43*, 1044–1056.

Zhu, Q., Li, J., Ma, J., Luo, M., Wang, B., Huang, H., Tian, X., Li, W., Zhang, S., Zhang, C., and Ju, J. (2012). Discovery and engineered overproduction of antimicrobial nucleoside antibiotic A201A from the deep-sea marine actinomycete *Marinactinospora thermotolerans* SCSIO 00652. Antimicrob. Agents Chemother. *56*, 110–114.

Molecular Cell, Volume *58*

Supplemental Information

Distinct tRNA Accommodation Intermediates Observed on the Ribosome with the Antibiotics Hygromycin A and A201A

Yury S. Polikanov, Agata L. Starosta, Manuel F. Juette, Roger B. Altman, Daniel S. Terry, Wanli Lu, Benjamin J. Burnett, George Dinos, Kevin A. Reynolds, Scott C. Blanchard, Thomas A. Steitz, and Daniel N. Wilson

I. SUPPLEMENTAL FIGURES AND MOVIES

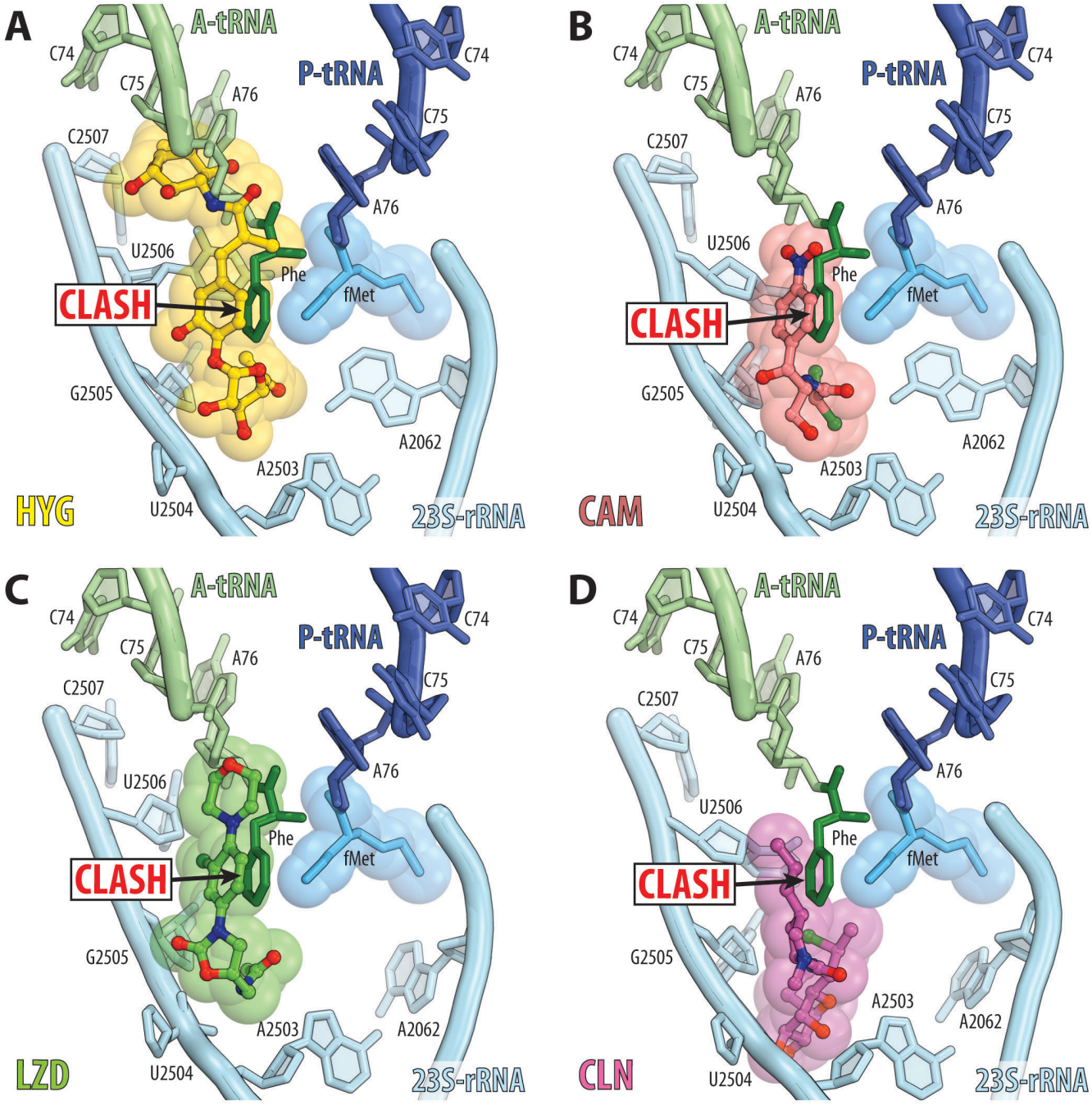

Figure S1, related to Figure 2. Comparison of antibiotic binding sites at the A site of the PTC. (**A-D**) Binding sites of (**A**) hygromycin A (HygA, yellow), (**B**) chloramphenicol (CAM, pink) (Bulkley et al., 2010; Dunkle et al., 2010), (**C**) linezolid (LZD, green) (Ippolito et al., 2008; Wilson et al., 2008) and (**D**) the lincosamide clindamycin (CLN, magenta) (Dunkle et al., 2010; Juette et al., 2014; Schlünzen et al., 2001) relative to Phe-tRNA in the A site (light green with Phe moiety coloured dark green) and fMet-tRNA in the P site (dark blue with fMet moiety coloured light blue) (Polikanov et al., 2014b). The 23S rRNA nucleotides are coloured cyan.

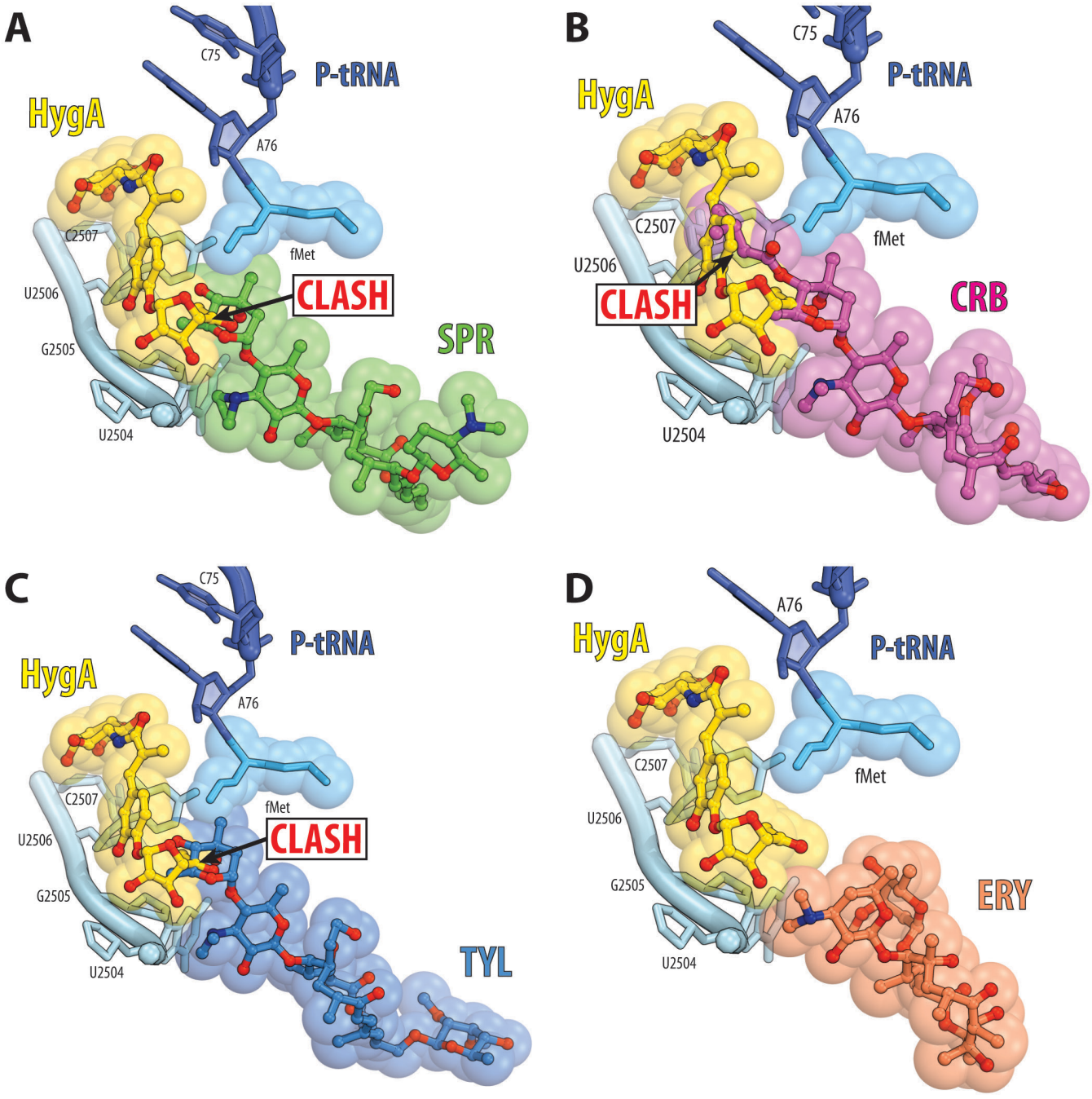

Figure S2, related to Figure 2. Comparison of HygA binding site with those of 16- and 14-membered macrolides. (**A-D**) Binding site of hygromycin A (HygA, yellow) relative to (**A**) spiramycin (SPR, green), (**B**) carbomycin A (CRB-A, magenta), (**C**) tylosin (TYL, blue) and (**D**) erythromycin (ERY, pink) (Bulkley et al., 2010; Dunkle et al., 2010; Hansen et al., 2002; Tu et al., 2005).

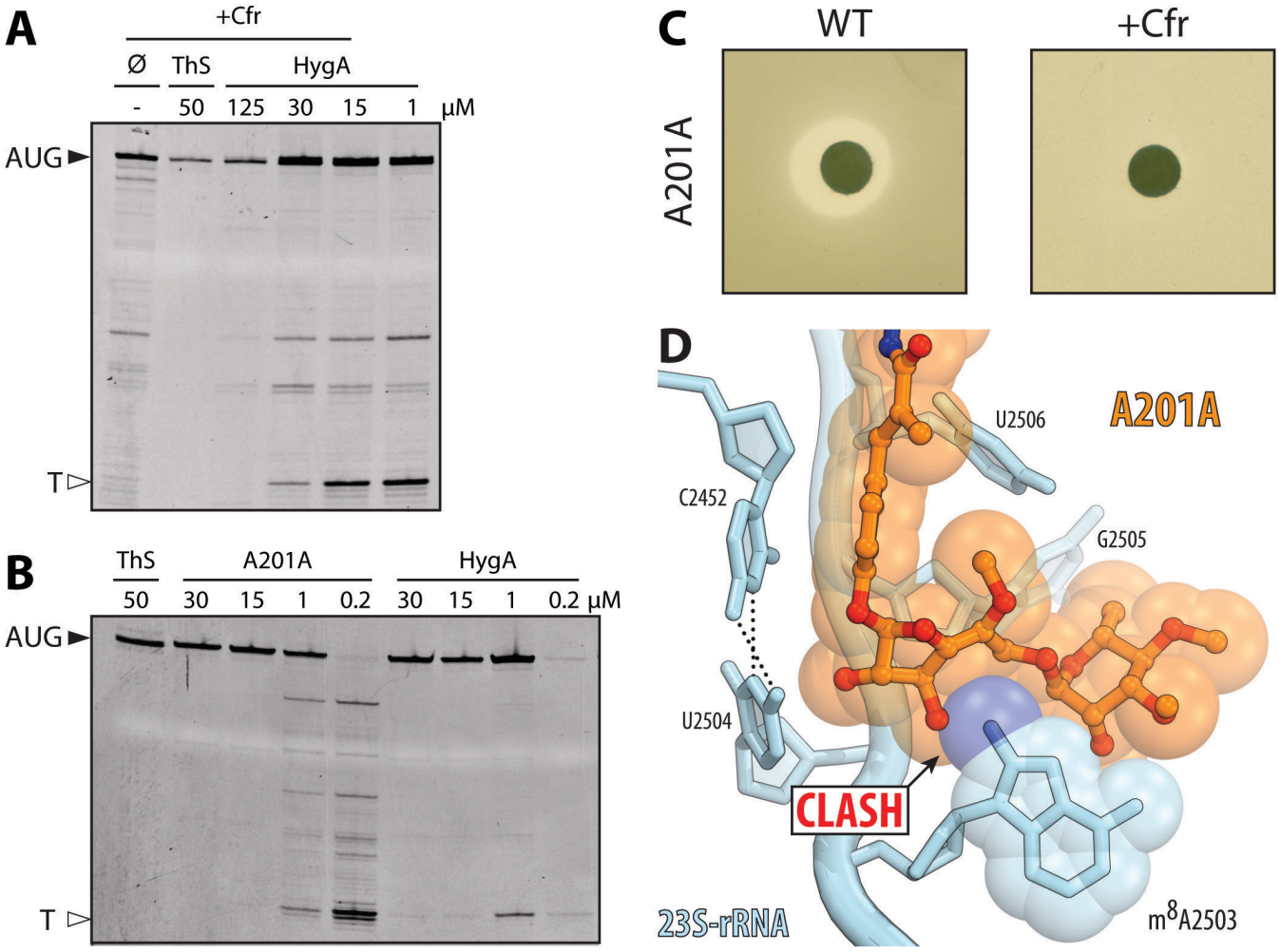

Figure S3, related to Figures 3 and 6. Resistance mechanisms for HygA and A201A. (**A**) Toe-printing assay monitoring translation on Cfr-modified ribosomes in the presence of increasing concentrations (1-125 μM) of HygA. (**B**) Toe-printing assay monitoring translation in the presence of increasing concentrations (0.2-30 μM) of A201A and HygA. In (A) and (B), the control reactions with thiostrepton (ThS) are shown. AUG designates location of the ribosomes stalled at the start codon, "T" denotes the position of the unique Thr codon, which stalls ribosomes because of the lack of Thr amino acid in the reaction mixture. (**C**) Disc-diffusion assay monitoring growth of wild-type *E. coli* strain lacking Cfr (WT, left) and same strain expressing Cfr (+Cfr, right) in the presence of A201A (5 nmol). (**D**) Molecular model of the C8 methylation of A2503 by Cfr, revealing a clash with the ribose of subunit A of HygA.

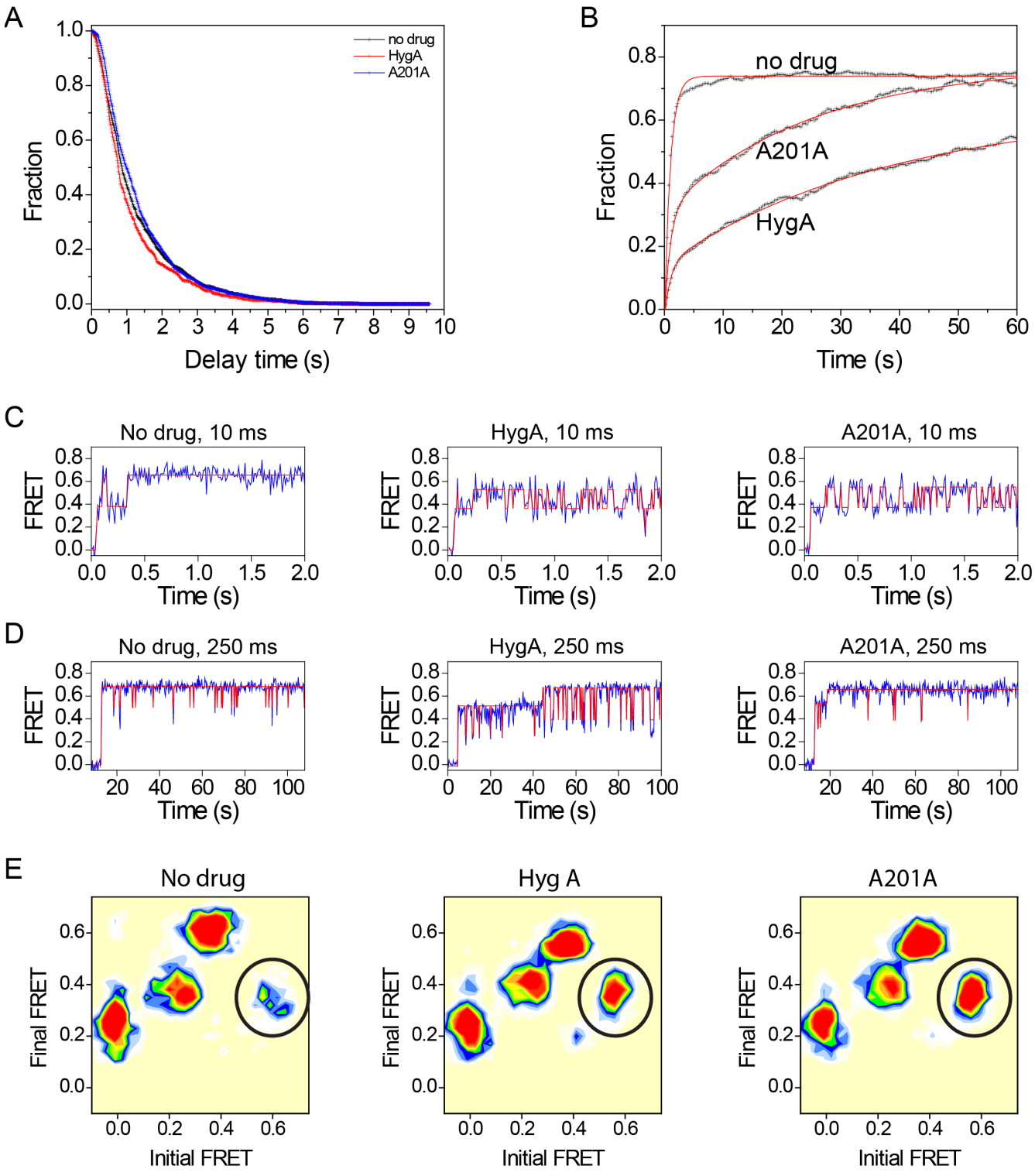

Figure S4, related to Figure 4. HygA and A201A specifically block A-tRNA progression through the proofreading phase of tRNA selection: (**A**) The bimolecular rate constant of A-tRNA binding to the ribosome and initial selection is unaffected by HygA and A201A as determined by the time delay between ternary complex mixing with the ribosome and the end of initial selection (intermediate FRET).

(**B**) Plot comparing the relative duration of intermediate FRET states during the uninhibited, HygA-stalled and A201A-stalled selection process. (**C**, **D**) HygA and A201A block the process of tRNA selection during proofreading, wherein aa-tRNA reversibly fluctuates between A/T-like and partially accommodated positions. (**C**) Repeated, futile attempts to complete the accommodation process are observed as rapid FRET fluctuations at fast (10 ms) time scale. While these sampling events occur even in the absence of drug (left panel; (Geggier et al., 2010)), the addition of HygA (middle panel) or A201A (right panel) prolongs the time window prior to full accommodation. (**D**) Longer time scale imaging (250 ms) was used to estimate the total duration of the drug-induced stall. (**E**) Transition density plots of the tRNA selection process highlight reversible fluctuations in the absence of drug (left) and in the presence of HygA (middle) or A201A (right). Each plot is a two-dimensional histogram of the FRET efficiencies observed immediately before and after transitions between different FRET-identified conformational states. Reversible transitions between intermediate- and high-FRET states that are present in uninhibited aa-tRNA selection and enhanced by HygA and A201A are highlighted in each TDP (black circles).

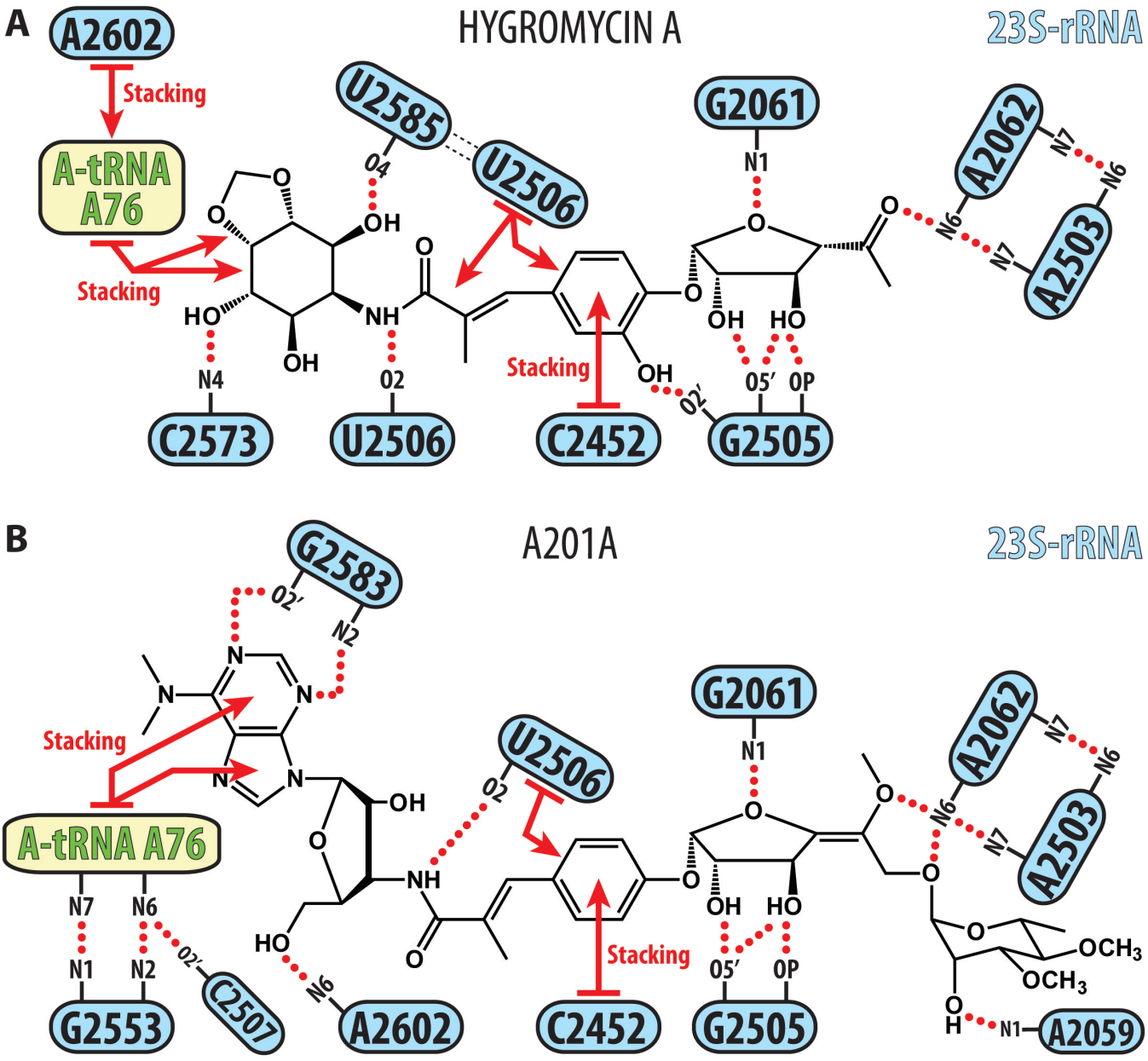

Figure S5, related to Figures 5 and 6. Schematic diagrams of interactions of HygA (A) and A201A (B) with the ribosome and A-tRNA. 23S rRNA nucleotides are highlighted in cyan and A76 of the A-tRNA is green. Potential H-bond interactions are indicated with dashed lines, stacking interactions are shown with arrows.

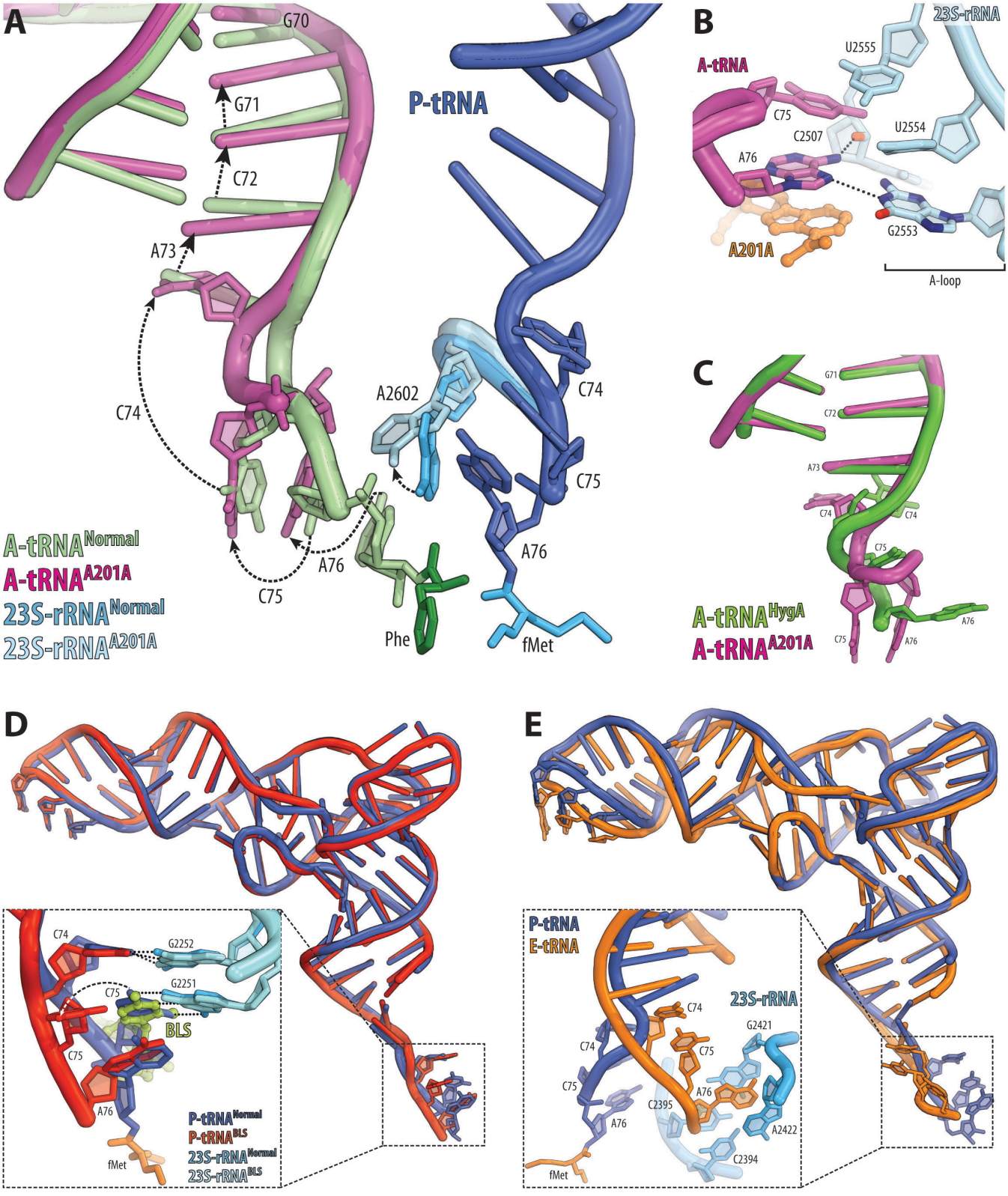

Figure S6, related to Figure 6. Partially accommodated A-tRNAs in the presence of A201A and known tRNA structures with non-stacking CCA-ends. (**A**) Comparison of the position of A-tRNA in the presence of A201A (magenta) with the canonical position of A-tRNA, when it is fully

accommodated in the A site (light green). Relative positions of A2602 in the presence (cyan) and absence (blue) of A201A are also shown. (**B**) Interactions of A76 of A-tRNA with G2553 and C2507 in the presence of A201A. (**C**) Comparison of the conformations of A-tRNA in the presence of HygA (green) and A201A (magenta). (**D**) Overview and zoom of the CCA-end of canonical P-tRNA (blue) involved in base-pairing interactions with G2251 and G2252 of the P-loop (H80) of the 23S rRNA (cyan) (Polikanov et al., 2014b) compared with the CCA-end of the P-tRNA (red) with flipped nucleotide C75 in the presence of the antibiotic blasticidin S (BLS, green) (Svidritskiy et al., 2013). (**E**) Overview and zoom of the CCA-end of $tRNA^{Phe}$ bound at the E site (orange) (Schmeing et al., 2003; Selmer et al., 2006) compared with the CCA-end of canonical A-tRNA (blue) aligned on the basis of the acceptor arms.

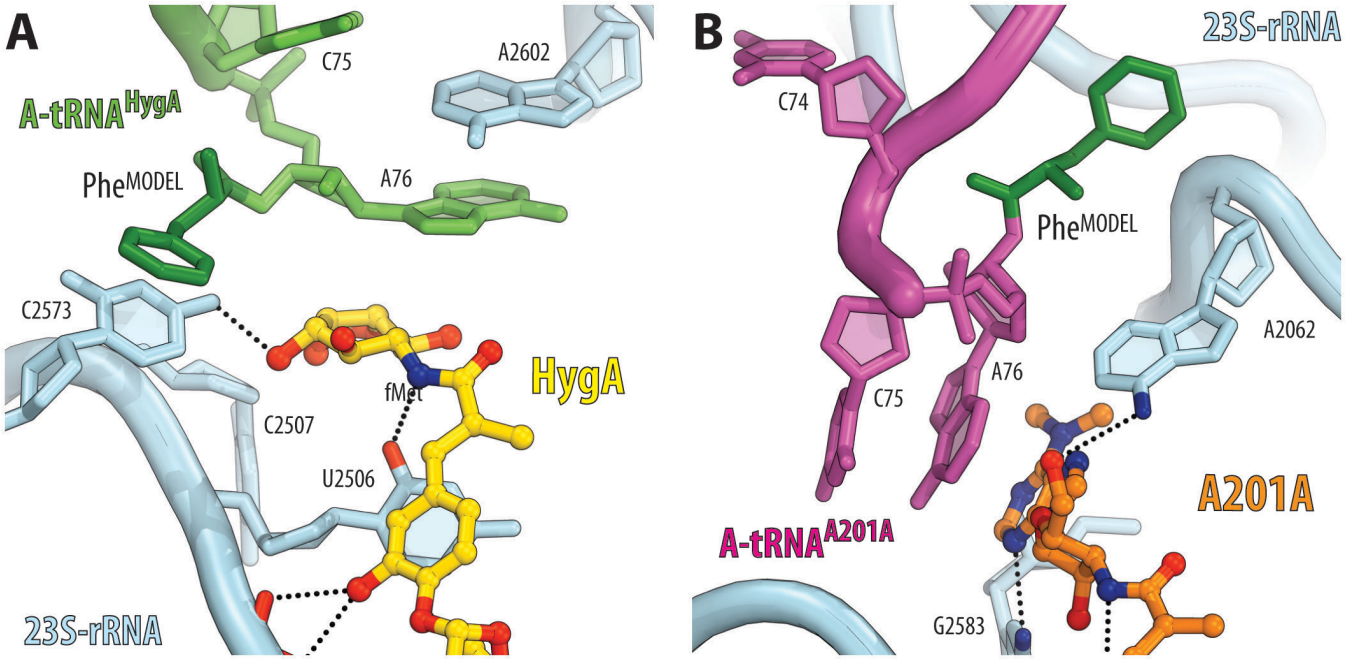

Figure S7, related to Figures 5 and 6. *In silico* modelling of Phe group onto partially accommodated A-tRNAs in the presence of hygromycin A (A) or A201A (B). Phe moiety is coloured in dark green, other colours are the same as in **Fig. 5B** and **Fig. 6E**, respectively.

Movie S1, related to Figure 5. Hygromycin A functional site in the 70S ribosome. The movie shows: (1) zoom-out and (2) close-up views of the HygA binding site in the large subunit of the *T. thermophilus* 70S ribosome programmed with mRNA and three tRNAs; (3) details of HygA interactions with the 23S rRNA in the A site of the ribosome; (4) unusual configuration of the CCA-end of the A-site tRNA (comparison of the position of A-tRNA in the presence of HygA with the canonical position of A-tRNA when fully accommodated in the A site); (5) stacking interactions between A76 of A-tRNA, A2602 and the aminocyclitol ring of HygA; (6) morph between the partially accommodated state of A-tRNA observed in the presence of HygA and the A/T-like state to illustrate oscillations between these two states which can occur for extended periods of time as observed by smFRET.

Movie S2, related to Figure 6. A201A functional site in the 70S ribosome. The movie shows: (1) zoom-out and (2) close-up views of the A201A binding site in the large subunit of the *T. thermophilus* 70S ribosome programmed with mRNA and three tRNAs; (3) details of A201A interactions with the 23S rRNA in the A site of the ribosome; (4) steric clash between the fucofuranose of A201A and the desosamine sugar of erythromycin; (5) unusual configuration of the CCA-end of the A-site tRNA (comparison of the position of A-tRNA in the presence of A201A with the canonical position of A-tRNA when fully accommodated in the A site); (6) non-canonical interactions between A76 of A-tRNA and G2553 of the A-loop of the 23S rRNA, which normally forms WC-interactions with the C75 of the A-site tRNA; (7) morph between the partially accommodated state of A-tRNA observed in the presence of HygA and the A/T-like state to illustrate oscillations between these two states which can occur for extended periods of time as observed by smFRET.

II. SUPPLEMENTAL EXPERIMENTAL PROCEDURES

1. *In vitro* translation assay

The inhibition of green fluorescent protein (GFP) synthesis by HygA, HygA~P or A201A was assessed using *E. coli* lysate-based transcription-translation coupled assay (RTS100, 5Prime) and as described previously (Starosta et al., 2010; Starosta et al., 2009). Briefly, 10 μL reactions with or without antibiotic were mixed according to the manufacturer's description and incubated for 3 hrs at 30°C. 2 μL of each reaction were diluted with 50 μL of buffer A (10 mM HEPES-KOH pH 7.8, 10 mM $MgCl_2$, 60 mM NH_4Cl, and 4 mM β-mercaptoethanol) and then transferred into black 96-well chimney flat bottom microtiter plate (Greiner). The GFP fluorescence was measured using a Tecan Infinite M1000 plate reader tuned to 395 nm/509 nm excitation/emission wavelengths. All measurements were repeated in triplicates and were characterized by standard deviation of less than 10%. Results were represented using SigmaPlot (Systat Software, Inc.).

2. Peptide bond formation assay

The peptidyltransferase activity in the presence or absence of antibiotic was measured using the puromycin reaction as described previously (Mamos et al., 2013). Briefly, 20 μL reactions of programmed ribosomal complexes containing 15 pmoles of ribosomes with P-site bound AcPhe-$tRNA^{Phe}$ were pre-incubated for 5 min at 30°C with an increasing amount of antibiotic in buffer B (20 mM HEPES-KOH pH 7.6, 150 mM $NH_4(CH_3COO)$, 4.5 mM $Mg(CH_3COO)_2$, 4 mM β-mercaptoethanol, 2 mM spermidine, 0.05 mM spermine). The reactivity of ribosomal complexes was monitored by addition of saturating amounts of puromycin (1 mM) in buffer B. Reactions were incubated for 3 min at 37°C and then stopped by the addition of equal volumes of 0.3 M sodium acetate pH 5.5 and extracted with 1 mL of ethyl acetate. Finally, the radioactivity of 700 μL of the organic phase containing N-Ac-Phe-puromycin complex was measured with a scintillation counter.

3. Erythromycin-binding assay

Binding of HygA, A201A and erythromycin (ERY) to an empty *E. coli* ribosome was monitored using a competition assay with radiolabelled [^{14}C]-erythromycin as described before (Karahalios et al., 2006; Petropoulos et al., 2009; Starosta et al., 2010). Briefly, 20 μL reactions containing 5 pmoles of ribosomes in buffer C (10 mM HEPES-KOH pH 7.8, 30 mM, $MgCl_2$, 150 mM NH_4Cl, and 6 mM β-mercaptoethanol) were pre-incubated with 1.25 μM of [^{14}C]-erythromycin (170 dpm/pmol), which resulted in binding of ERY to 60% of the ribosomes according to the saturation curve (data not shown). To assess binding of other antibiotics, ribosomal complex with ERY was incubated with increasing

amounts of either HygA or A201A for 2 hrs at room temperature. Reactions were passed through HA-type 0.45 mm pore size nitrocellulose filters (Merck Millipore). Filters were washed three times with buffer C and then scintillation counted in the presence of Filtersafe scintillant (Zinsser Analytic).

4. Toe-printing assay

The position of the ribosome on the mRNA was monitored using a toe-printing assay based on the *in vitro* coupled transcription-translation system using the PURExpress Δaa ΔtRNA kit (New England Biolabs) as described previously (Starosta et al., 2014). For experiments using Cfr-modified ribosomes, the PURExpress Δaa ΔtRNA Δribosome kit (New England Biolabs) was used and Cfr-modified ribosomes were substituted in place of wildtype *E. coli* 70S ribosomes. Briefly, 2.5 μL reactions with template DNA (5'-TTAATACGACTCACTATAGGGGAATTGTGAGCGGATAACAATTCCCCTCTAGAAATAATTTTGTTTAACTTTAAGAAGGAGATATACAT**ATGCATCATCATCATCATCACAAGAATATACGTAACTTTTCGATCATAGCTCACATTGACCACCTGCCGTTTACCTAATAA**GAGCTCGGTAAATCGACGCTGTCTGACCGTATTATCCAGATCTGCGGTGGCCTGTCTGACCGTGAAATGGAGGCGCAGGTTCTC-3'; ORF is highlighted by underlined and bold text) were supplemented with a FAM-labeled primer (5'-GAGAACCTGCGCCTCCATTTCACGGTC-3') and amino acid mixture lacking threonine and then incubated for 30 min at 37°C in the presence or absence of antibiotics. Reverse transcription reaction was primed by addition of 100 units of Superscript III reverse transcriptase (Life Technologies) and dNTP mixture to the final concentration of 400 μM, and was carried out for an additional 30 min at 37°C. Products of the reactions were purified using Nucleotide Removal Kit (Qiagen) and lyophilized. Pellets were resuspended in formamide loading dye solution and applied to 6% acrylamide gel (19:1) containing 7M urea. Fluorescence of the samples was detected using a Typhoon FLA9500 scanner. Intensity of stalled bands was acquired using ImageJ software. Thiostrepton (100 μM) was used as a positive control for inhibition of translation initiation, while lack of threonine in the amino acid mixture was used to stall ribosomes during translation elongation.

5. Single molecule FRET imaging

All experiments were performed in Tris-polymix buffer containing 50 mM Tris-acetate pH 7.5, 5 mM $Mg(CH_3COO)_2$, 100 mM KCl, 5 mM $NH_4(CH_3COO)$, 0.5 mM $CaCl_2$, 0.1 mM EDTA, 5 mM putrescine, 1 mM spermidine, 1.5 mM β-mercaptoethanol, and 1 mM GTP, in the presence of an oxygen scavenging environment (2 mM protocatechuic acid (PCA), 50 nM protocatechuate 3,4-dioxygenase (PCD) and a cocktail of triplet-state quenching compounds (1 mM Trolox, 1 mM cyclooctatetraene,

1 mM nitrobenzyl-alcohol) (Dave et al., 2009). The ternary complex of EF-Tu•GTP•Phe-tRNA^{Phe}(Cy5-acp^{3}U47) was prepared following the established procedures (Blanchard et al., 2004; Munro et al., 2007). To increase the FRET imaging duration and overall signal-to-noise ratio of imaging, an intramolecularly photostabilized derivative of Cy5 was employed in combination with a cocktail of solution protective agents (Juette et al., 2014; Zheng et al., 2014). Ribosome complexes (0.5 nM) programmed with biotinylated mRNA were surface immobilized by brief incubation within PEG-passivated, streptavidin-coated quartz microfluidic devices (Munro et al., 2007). In order to minimize the contribution of hybrid state tRNA configurations formed after peptide bond formation, experiments were performed using complexes lacking ribosomal protein L1 (Munro et al., 2007).

smFRET data were acquired using a home-built prism-based total internal reflection (TIR) microscope as previously described (Munro et al., 2007). The Cy3 fluorophore linked to tRNA^{fMet} was excited by the evanescent wave generated by total internal reflection of a single frequency light source (Opus 532 nm, Laser Quantum). Photons emitted from both Cy3 and Cy5 were collected using a 1.27 NA 60X water-immersion objective (Nikon) and a dichroic filter (T635lpxr, Chroma) was used to spatially separate Cy3 and Cy5 fluorescence. Fluorescence data were acquired with integration times of 10 ms or 250 ms. FRET trajectories were calculated from fluorescence traces using the formula $FRET=I_{Cy5}/(I_{Cy3}+I_{Cy5})$, where I_{Cy3} and I_{Cy5} represent the Cy3 and Cy5 fluorescence intensities, respectively. Fluorescence and FRET traces were selected for analysis using semi-automated smFRET analysis software implemented in Matlab (The MathWorks) as previously described (Geggier et al., 2010).

6. Crystallographic structure determination

Ribosome complexes with mRNA and tRNAs were formed by programming of 5 μM *Tth* 70S ribosomes with 10 μM mRNA and incubation at 55°C for 10 min, followed by addition of 20 μM P-site (fMet-tRNA$_i^{Met}$) and 20 μM A-site (Phe-tRNA^{Phe}) substrates (with minor changes from (Voorhees et al., 2009)). Each of the last two steps was allowed to reach equilibrium for 10 min at 37°C. In the co-crystallization experiments with either HygA or A201A, the antibiotic was added to a final concentration of 100 μM, and the complex was left at room temperature for an additional 15 min prior to crystallization. All *Tth* 70S ribosome complexes were formed in the buffer containing 5 mM HEPES-KOH (pH 7.6), 50 mM KCl, 10 mM NH_4Cl, and 10 mM $Mg(CH_3COO)_2$, and then crystallized in the buffer containing 100 mM Tris-HCl (pH 7.6), 2.9% (w/v) PEG-20K, 7-12% (v/v) MPD, 100-200 mM arginine, 0.5 mM β-mercaptoethanol. Crystals were grown by the vapor diffusion method in sitting drops at 19°C and stabilized as described previously (Polikanov et al., 2012; Polikanov et al., 2014a)

with the antibiotics included in the stabilization buffers (100 μM HygA or 100 μM A201A). Diffraction data were collected using beamline 24ID-C at the Advanced Photon Source and beamline X25 at the Brookhaven National Laboratory. All crystals belonged to the primitive orthorhombic space group $P2_12_12_1$ with approximate unit cell dimensions of 210Å x 450Å x 620Å and contained two copies of the 70S ribosome per asymmetric unit. Each structure was solved by molecular replacement using PHASER from the CCP4 program suite (McCoy et al., 2007). The search model was generated from the previously published structure of *T. thermophilus* 70S ribosome with bound mRNA and tRNAs (PDB entries 4QCM/4QCN from (Polikanov et al., 2014b)). The initial molecular replacement solutions were refined by rigid body refinement with the ribosome split into multiple domains, followed by positional and individual B-factor refinement. The final models of the 70S ribosome in complex with HygA and with or without mRNA/tRNAs, as well as the A201A complex with 70S ribosome and mRNA/tRNAs were generated by multiple rounds of model building in COOT (Emsley and Cowtan, 2004), followed by refinement in PHENIX (Adams et al., 2010). The statistics of data collection and refinement for each complex are compiled in **Table 1**.

III. SUPPLEMENTAL REFERENCES

Adams, P.D., Afonine, P.V., Bunkoczi, G., Chen, V.B., Davis, I.W., Echols, N., Headd, J.J., Hung, L.W., Kapral, G.J., Grosse-Kunstleve, R.W., *et al.* (2010). PHENIX: a comprehensive Python-based system for macromolecular structure solution. Acta Crystallogr. D Biol. Crystallogr. *66*, 213-221.

Blanchard, S.C., Gonzalez, R.L., Kim, H.D., Chu, S., and Puglisi, J.D. (2004). tRNA selection and kinetic proofreading in translation. Nat. Struct. Mol. Biol. *11*, 1008-1014.

Bulkley, D., Innis, C.A., Blaha, G., and Steitz, T.A. (2010). Revisiting the structures of several antibiotics bound to the bacterial ribosome. Proc. Natl. Acad. Sci. USA *107*, 17158-17163.

Dave, R., Terry, D.S., Munro, J.B., and Blanchard, S.C. (2009). Mitigating unwanted photophysical processes for improved single-molecule fluorescence imaging. Biophys. J. *96*, 2371-2381.

Dunkle, J.A., Xiong, L., Mankin, A.S., and Cate, J.H. (2010). Structures of the *Escherichia coli* ribosome with antibiotics bound near the peptidyl transferase center explain spectra of drug action. Proc. Natl. Acad. Sci. USA *107*, 17152-17157.

Emsley, P., and Cowtan, K. (2004). Coot: model-building tools for molecular graphics. Acta Crystallogr. D Biol. Crystallogr. *60*, 2126-2132.

Geggier, P., Dave, R., Feldman, M.B., Terry, D.S., Altman, R.B., Munro, J.B., and Blanchard, S.C. (2010). Conformational sampling of aminoacyl-tRNA during selection on the bacterial ribosome. J. Mol. Biol. *399*, 576-595.

Hansen, J.L., Ippolito, J.A., Ban, N., Nissen, P., Moore, P.B., and Steitz, T.A. (2002). The structures of four macrolide antibiotics bound to the large ribosomal subunit. Mol. Cell *10*, 117-128.

Ippolito, J.A., Kanyo, Z.F., Wang, D., Franceschi, F.J., Moore, P.B., Steitz, T.A., and Duffy, E.M. (2008). Crystal structure of the oxazolidinone antibiotic linezolid bound to the 50S ribosomal subunit. J. Med. Chem. *51*, 3353-3356.

Juette, M.F., Terry, D.S., Wasserman, M.R., Zhou, Z., Altman, R.B., Zheng, Q., and Blanchard, S.C. (2014). The bright future of single-molecule fluorescence imaging. Curr. Opin. Chem. Biol. *20*, 103-111.

Karahalios, P., Kalpaxis, D.L., Fu, H., Katz, L., Wilson, D.N., and Dinos, G.P. (2006). On the mechanism of action of 9-O-arylalkyloxime derivatives of 6-O-mycaminosyltylonolide, a new class of 16-membered macrolide antibiotics. Mol. Pharmacol. *70*, 1271-1280.

Mamos, P.L., Krokidis, M.G., Papadas, A.T., Karahalios, P., Starosta, A.L., Wilson, D.N., Kalpaxis, D.L., and Dinos, G.P. (2013). On the use of the antibiotic chloramphenicol to target polypeptide chain mimics to the ribosomal exit tunnel. Biochemie, in press.

McCoy, A.J., Grosse-Kunstleve, R.W., Adams, P.D., Winn, M.D., Storoni, L.C., and Read, R.J. (2007). Phaser crystallographic software. J. Appl. Crystallogr. *40*, 658-674.

Munro, J.B., Altman, R.B., O'Connor, N., and Blanchard, S.C. (2007). Identification of two distinct hybrid state intermediates on the ribosome. Mol. Cell *25*, 505-517.

Petropoulos, A.D., Kouvela, E.C., Starosta, A.L., Wilson, D.N., Dinos, G.P., and Kalpaxis, D.L. (2009). Time-resolved binding of azithromycin to *Escherichia coli* ribosomes. J. Mol. Biol *385*, 1179-1192.

Polikanov, Y.S., Blaha, G.M., and Steitz, T.A. (2012). How hibernation factors RMF, HPF, and YfiA turn off protein synthesis. Science *336*, 915-918.

Polikanov, Y.S., Osterman, I.A., Szal, T., Tashlitsky, V.N., Serebryakova, M.V., Kusochek, P., Bulkley, D., Malanicheva, I.A., Efimenko, T.A., Efremenkova, O.V.*, et al.* (2014a). Amicoumacin A inhibits translation by stabilizing mRNA interaction with the ribosome. Mol. Cell *56*, 531-540.

Polikanov, Y.S., Steitz, T.A., and Innis, C.A. (2014b). A proton wire to couple aminoacyl-tRNA accommodation and peptide-bond formation on the ribosome. Nat. Struct. Mol. Biol. *21*, 787-793.

Schlünzen, F., Zarivach, R., Harms, J., Bashan, A., Tocilj, A., Albrecht, R., Yonath, A., and Franceschi, F. (2001). Structural basis for the interaction of antibiotics with the peptidyl transferase center in eubacteria. Nature *413*, 814-821.

Schmeing, T.M., Moore, P.B., and Steitz, T.A. (2003). Structures of deacylated tRNA mimics bound to the E site of the large ribosomal subunit. RNA *9*, 1345-1352.

Selmer, M., Dunham, C.M., Murphy, F.V.t., Weixlbaumer, A., Petry, S., Kelley, A.C., Weir, J.R., and Ramakrishnan, V. (2006). Structure of the 70S ribosome complexed with mRNA and tRNA. Science *313*, 1935-1942.

Starosta, A.L., Karpenko, V.V., Shishkina, A.V., Mikolajka, A., Sumbatyan, N.V., Schluenzen, F., Korshunova, G.A., Bogdanov, A.A., and Wilson, D.N. (2010). Interplay between the ribosomal tunnel, nascent chain, and macrolides influences drug inhibition. Chem. Biol. *17*, 1-10.

Starosta, A.L., Lassak, J., Peil, L., Atkinson, G.C., Virumae, K., Tenson, T., Remme, J., Jung, K., and Wilson, D.N. (2014). Translational stalling at polyproline stretches is modulated by the sequence context upstream of the stall site. Nucleic Acids Res. *42*, 10711-10719.

Starosta, A.L., Qin, H., Mikolajka, A., Leung, G.Y., Schwinghammer, K., Nicolaou, K.C., Chen, D.Y., Cooperman, B.S., and Wilson, D.N. (2009). Identification of distinct thiopeptide-antibiotic precursor lead compounds using translation machinery assays. Chem. Biol. *16*, 1087-1096.

Svidritskiy, E., Ling, C., Ermolenko, D.N., and Korostelev, A.A. (2013). Blasticidin S inhibits translation by trapping deformed tRNA on the ribosome. Proc. Natl. Acad. Sci. USA *110*, 12283-12288.

Tu, D., Blaha, G., Moore, P.B., and Steitz, T.A. (2005). Structures of MLSBK antibiotics bound to mutated large ribosomal subunits provide a structural explanation for resistance. Cell *121*, 257-270.

Voorhees, R.M., Weixlbaumer, A., Loakes, D., Kelley, A.C., and Ramakrishnan, V. (2009). Insights into substrate stabilization from snapshots of the peptidyl transferase center of the intact 70S ribosome. Nat. Struct. Mol. Biol. *16*, 528-533.

Wilson, D.N., Schluenzen, F., Harms, J.M., Starosta, A.L., Connell, S.R., and Fucini, P. (2008). The oxazolidinone antibiotics perturb the ribosomal peptidyl transferase center and effect tRNA positioning. Proc. Natl. Acad. Sci. USA *105*, 13339-13344.

Zheng, Q., Juette, M.F., Jockusch, S., Wasserman, M.R., Zhou, Z., Altman, R.B., and Blanchard, S.C. (2014). Ultra-stable organic fluorophores for single-molecule research. Chem. Soc. Rev. *43*, 1044-1056.